A Publication of the AIMS South Africa Research Centre

# ARC REPORT

2020

AIMS African Institute for Mathematical Sciences SOUTH AFRICA

# Contents

# Editor's Note

*Prof. Barry Green, Director*

Welcome to the latest edition of the ARC Report.

The Research Centre at AIMS South Africa is normally a vibrant active place. Researchers and visitors spend most of their time there, from mid-morning until late at night. Offices are shared, often with three visiting researchers in the same office. Blackboards are filled with formulae and math arguments. There are tea-time discussions, seminars a journal club, workshops and Postdocs, PhD and Research Masters students working on projects. They are around and all wander across the road from the AIMS Research Centre to our Main Building to have lunch with the rest of the AIMS family, roughly 120 people, on any weekday. The many workshops organised bring local and international scientists and students together, so that the atmosphere is even more lively and focussed, and all have the feeling this is a special worthwhile place to be.

Now it is all virtual, COVID 19 has jolted us, as it has every other facet of life worldwide. No science, or science in silence might be what one expects, but fortunately, I think without realising this much, in many essential ways to scientific life we were prepared to cope with this. Although virtual environments and activities cannot replace the hum of people working together in groups, it has meant one has still been able to share work done, hold discussions with each other and students, connect to those far away, and extend the time one would normally spend alone or in small groups thinking about problems, to activities normally face to face, but now with a laptop connecting to the group.

Researchers at AIMS are working on and have contributed to a number of interesting problems, some very relevant to the situation we find ourselves in at present. This report presents some of their work, which gives a picture of what has been done in the ARC recently, especially since lockdown. It is a pleasure to thank all who have contributed. We hope those reading will enjoy finding out what our colleagues and research students have been doing, which may lead to interaction too.


**In light of the crisis caused by the Coronavirus, a few of our researchers have taken the opportunity to conduct research into various aspects of the disease and its implications.**

# NNLAD algorithm for robust COVID-19 testing

*Authors: Hendrik Petersen, Bubacarr Bah, Peter Jung*

In compressed sensing the goal is to recover a signal from as few as possible noisy, linear measurements.The general assumption is that the signal has only a few non-zero entries. Given an estimate for the noise level a common convex optimization approach, Basis Pursuit (BP) De-noising (BPDN) is used to recover the signal. In the case of unknown noise levels, non-negative least squares (NNLS) recovers non-negative signals if the measurement matrix fulls some properties. However, if the measurement matrix is an expander matrix or a bi-adjacency matrix of a random left regular bipartite graph, we denote as D-LRBG, it fails to obey some of these properties. In this setting $\ell_1$-constrained least residual (CLR) could be used. However, we propose a non-negative least absolute deviation (NNLAD), see (3). For these measurement matrices, we prove a uniform, stable and robust recovery guarantee with NNLAD. Such guarantees are important, since binary expander matrices are sparse and thus allow for fast sketching and recovery. Our implementation of the NNLAD shows that this is comparable to state of the art methods. Coincidentally, NNLAD can be used for group testing, which is necessary in the recent COVID-19 crisis, where contamination of specimens may be modelled as peaky (or sparse) noise. We argue that the lack of knowledge of the noise in such testing favours the NNLAD recovery method over a BPDN approach. Further, since the total sum of viruses in all patients is unknown, it is undesirable to use CLR.

With the outbreak and rapid spread of the COVID-19 virus, we are in the need of testing a lot of people for an infection. Since we can only test a fixed number of persons in a given time, the number of persons tested for the virus grows at most linearly. On the other hand, models suggest that the number of possibly infected persons grows exponentially. At some point, if that is not already the case, we will have a shortage of test kits and we will not be able to test every person. It is thus desirable, to test as much persons with as few as possible test kits. The field *group testing* develops strategies to test groups of individuals instead of individuals in order to reduce the amount of tests required to identify individuals with a certain property. The first advances in group testing were made by Dorfman in 1943.

The problem of testing a large group for a virus can be modeled as a compressed sensing problem in the following way. Suppose we want to test $N$ persons, labelled by $[N]=\{1,...,N\}$, to check whether or not they are affected by a virus. We denote by $x_n + e_n^{spe}$ the quantity of viruses in the specimen of the $n$-th person, where $x_n$ is the amount of viruses originating from the test person and $e_n^{spe}$ is a the quantity of viruses originating from a possible contamination of the specimen. Suppose we have $M$ test kits, labelled by $[M] = \{1,...,M\}$, typically $M < N$. By $y_m$ we denote the amount of viruses in the sample of the $m$-th test kit. Consider an $MxN$ matrix, $\mathbf{A}\in [0; 1]^{M\times N}$. For every $n$ we put a fraction of size $A_{m,n}$ of the specimen of the $n$-th person into the sample for the $m$-th test kit. The sample of the $m$-th test kit will then have the quantity of viruses

$$y_m = \sum_{n\in[N]} A_{m,n}\,(x_n + e_n^{spe}) + e_m^{pro}, \tag{1}$$

where $e^{pro}$ is the amount of viruses in the sample from a possible contamination of the sample. Usually, when using a test kit the viruses are duplicated multiple times, for instance with a polymerase chain reaction. The test kit will then detect a known, bijective transformation of each individual component $y_m$. Hence, we can calculate $y_m$ directly and thus assume that $y_m$ is the result of the test. After all $M$ tests we detect the quantity

$$\mathbf{y} = \mathbf{Ax} + \mathbf{e}, \tag{2}$$

where $\mathbf{y}$ and $\mathbf{e} = \mathbf{A}\mathbf{e}^{spec} + \mathbf{e}^{pro}$ are $M$-dimensional vectors and $\mathbf{x}$ is an $N$-dimensional vector. For now we assume that $\mathbf{e}$ is peaky and we will later argue why such a model is natural to assume.

Often each specimen is tested separately, meaning that A is the identity. In particular, we need at least as much test kits as specimens. Further, we estimate the true quantity of viruses $x_n$ by $x_n^{\#} := y_n$, which results in the estimation error $x_n - x_n^{\#} = e_n = e_n^{spe} + e_n^{pro}$. In this scenario the estimation error for the $n$-th person is only affected by the errors made while taking its specimen and testing its sample. Since the noise vector $\mathbf{e}$ is peaky, some but few tests will be inaccurate and might result in false positives or false negatives. In general, only a fraction of persons is indeed affected by the virus. Thus, we assume this number is less than $S$, for some small $S$. Since the amount of viruses is a non-negative value, we also have $\mathrm{x} \geq 0$. Our theory suggests to choose A as an expander matrix or to choose A as a $D$-LRBG matrix. Such a matrix A has non-negative entries and the column sums of A are not greater than one. This is a necessary requirement since each column sum is the total amount of specimen used in the test procedure. Precisely, a fraction of $D^{-1}$ of each specimen is used in exactly $D$ test kits.

In order to calculate an estimation to the true quantity of viruses x we propose to use the NNLAD. To be precise the NNLAD solution is given by

$$\mathrm{x}^{\#} = \underset{\mathrm{z}\geq 0}{\operatorname{argmin}} \,\|\, \mathrm{Az} - \mathrm{y} \,\|_1 \tag{3}$$

Our theory shows that this allows us to reduce the number of test kits required to $M = CS \log(N/S)$ for some constant $C$. Further, as we have seen in Figure 1, the approximation error is incredibly small since the noise e is peaky. In this manner, the estimation will even be more exact than by testing each specimen separately.

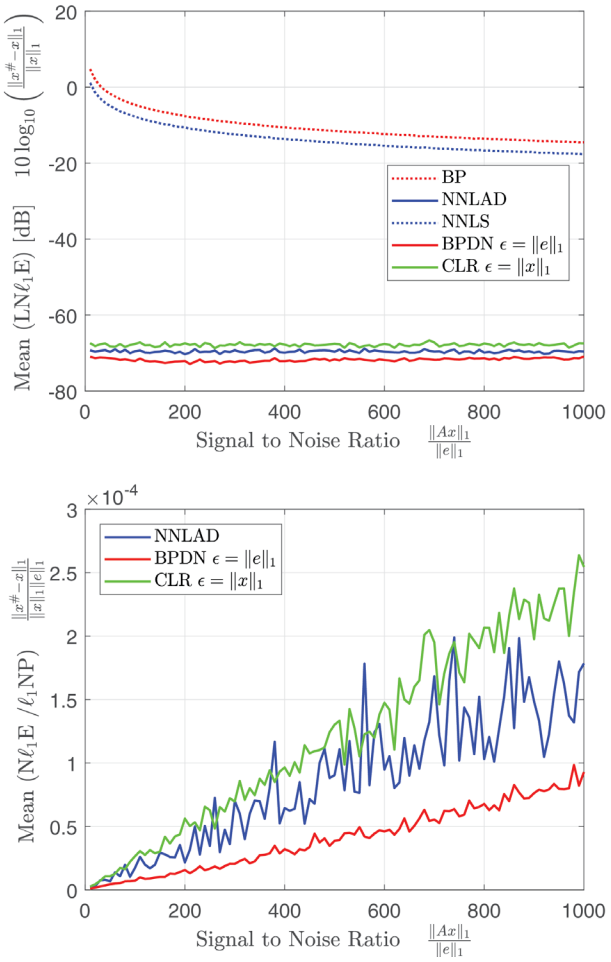


*Figure 1: Performance of NNLAD for noise with peaky mass and varying noise power. Top: The NNLAD outperforms the NNLS. Bottom: The estimation error does not scale linearly with the noise power.*

It remains to argue, why a peaky noise model is natural for the problem of testing a large group for a virus. In general, the sample of the $m$-th test kit will be affected by the noise $e_m^{pro} \neq 0$ if for instance the sample is contaminated by a specimen of a different person or a laboratory employee. Due to the caution and expertise of members in the health care system, this is a rare occasion, but when it happens the effect will be rather strong. Thus, it is natural to assume that $\mathbf{e}^{pro}$ is peaky. Similarly, the specimen of the $n$-th person is affected by the noise $e_n^{spe}$ under similar circumstances. Thus, it is also natural to assume that $\mathbf{e}^{spe}$ is peaky.

If we test each specimen separately it follows that $\mathbf{e} = \mathbf{e}^{spe} + \mathbf{e}^{pro}$ is peaky. On the other hand if $\mathbf{A}$ is a $D$-LRBG, the sample of the $m$-th test kit is affected by the noise of the $n$-th specimen if and only if $A_{m,n} \neq 0$. Since, there are exactly $D$ non-zeros per column, exactly $D$ samples are affected by the noise of the $n$-th specimen, i.e. by $D^{-1}e_n^{spe}$. If $n_e$ denotes the number of components of $\mathbf{e}^{spe}$ with signicant absolute value and $m_e$ denotes the number of components of $\mathbf{e}^{pro}$ with signicant absolute value, then the number of components of $\mathbf{e}$ with signicant absolute value is at most $Dn_e + m_e$. If $D$ is sufficiently small, as it is required the noise will be peaky.

# Long Term COVID-19 Forecasts for South Africa

*Authors: Richard Armstrong, Bruce Bassett, Nadeem Oozeer and Felix Silwimba; as part of the SARAO Data Science team's work for the National Ventilator Project.*

*"All models are wrong, but some are useful"* - George Box, British statistician

Predicting deaths from COVID-19 is hard: in the first few days of June 2020, the disease had killed 45 people in Qatar but 9522 in Belgium, yet Qatar - with 62,160 infections - had about 3500 more cases than Belgium. That is a ratio of about 200:1 in deaths, yet both countries had tested about 80,000 people per million of the population.

Predicting future COVID deaths is hard; or as Koos Bekker recently opined about general COVID-19 forecasts, "Only mamparas will try to predict the outcome of catastrophes."

With this in mind how many deaths should we expect in South Africa, and how accurately do we think that anyone can predict the final death toll? There have been optimistic suggestions that the total number of deaths will be low: in particular claims of 59,300 (here), 48,000 here and 30,000-50,000 (here; though the latter, for example, included many caveats about unmodelled uncertainties). If these projections turn out to be true it would be great news given that early projections were that over 300,000 South Africans might die, so let's indeed hope they turn out to be correct.

Unfortunately unjustified hope can be negative. The low death forecasts may give the impression that COVID-19 is guaranteed to only kill a relatively small number of South African's no matter what the public or government do for the rest of 2020 and 2021. One might be tempted to argue that if less than 50,000 people are going to die no matter what, then why should one bother to social distance, wear a mask or work from home?

Instead in this article we will attempt to convince you that:

1. it is currently impossible to predict the final death toll with any accuracy, and
2. it is still very possible that there will be more than 100,000 total deaths in South Africa over the next two years from COVID-19. Further, the original 300,000+ death toll must still be considered a realistic possibility.

Before we get into serious modelling let's start by addressing an argument that goes something like this:

*"How can we expect over 100,000 deaths in South Africa when Italy/Spain/(insert your favourite 1st world country) have only had 34,000/27,000/etc... deaths and they have been hit much harder than us?"*

The counter to this is straight-forward. First, South Africa is not a 1st world country and is no stranger to massive infectious disease death tolls: HIV deaths alone were estimated to exceed 250,000 a year for several years around 2006, and HIV is still a massive cause of death today. Further, our lockdown has not managed to bring the spread of the disease under control as it did in the first world: on 14th June we had the highest percentage of new cases in the world.

Second, let's wait and see what the total deaths in Italy/Spain/your favourite country are in January 2021 or 2022. History is full of sports matches where teams who were winning in the first quarter ended up losing badly by the end of the match. We simply don't yet know how long COVID-19 is going to be with us. It could be months if we develop effective treatments or a vaccine quickly, or it might last years if we don't. While the disease is with us, we should expect multiple waves of infections. As an example, have a look at daily cases in Iran who are just going through their second wave:

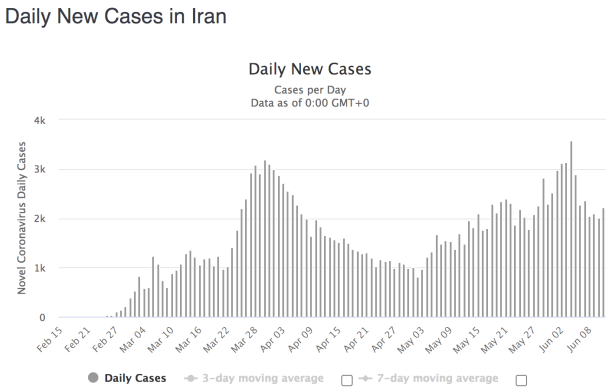


Iran is not alone in experiencing a 2nd wave: we must not forget just how extremely infectious COVID-19 is.

The fact that we don't really have any idea how long COVID-19 will be with us should already suggest that accurate long-term predictions are going to be difficult to make. If this sounds hard to believe, please reread the opening lines of this article and try to imagine predicting the Qatar and Belgium deaths today back in early March when both countries had less than 5 known cases each. As was this example, we will try to convince you that we cannot now predict the eventual number of deaths in South Africa that will occur over the next two years to better than about 50x. In other words, 10,000 and 500,000 deaths, and everything in between, are still possible final death tolls for South Africa due to COVID-19. Such long-tails are a known issue for epidemics.

This huge uncertainty is a bitter pill to swallow, so we invite you to stay critical, but open minded, while we work through the evidence.

**Understanding the original predictions**
First let's understand where the original predictions of around 300,000 deaths came from and why they are pretty robust.

Predicting final deaths for a disease is easy in principle: you just multiply the average Infection Fatality Rate (IFR; the probability of dying given infection) by the final total number of infections in the country: if 1 out of 100 people dies on average, and 100,000 people get infected, we would expect 1,000 people to die.

So how many infections should we expect in total in South Africa? The standard epidemiological answer to this is provided by the following curve which gives the final "herd immunity" fraction of infections in the population:

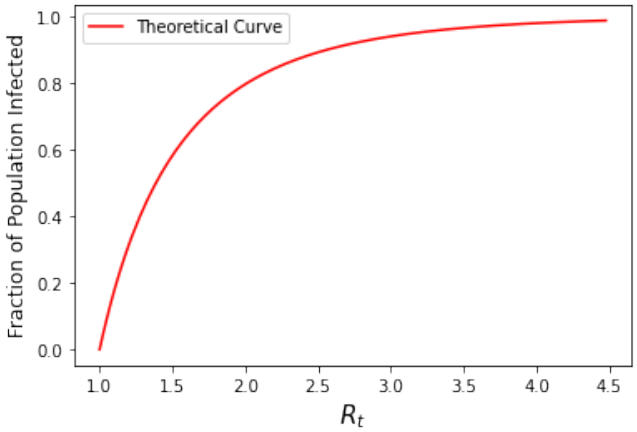


*Figure 1: predicted fraction of population infected as a function of reproductive number, Rt. It predicts about 60% of the population will be infected if Rt = 1.5 and about 80% infections for Rt = 2.*

Figure 1 links the proportion of the population who are expected to be infected given enough time to the reproductive number, Rt, a crucial quantity that we will need for all our forecasts. Rt is defined to be the average number of people an infected person will in turn pass the infection on to (think of John infecting Bob, Mary and Sizwe, yielding Rt = 3). It is important to note that the reproductive number is an average and that it changes with time, so it is useful to distinguish its initial value (R0 - when it starts spreading and no one knows about the disease) and its value at a later time, t, denoted by Rt. The value of R0 can be more than 10 for some diseases like the measles or mumps and is around 0.9-2.1 for influenza.

So for flu you usually infect just 1-2 other people but for COVID-19 R0 is estimated to be between about 2 and 6, so looking at Figure 1 we see that if nothing were done, we would expect at least 80% of any population to become infected with COVID-19 before the disease naturally stopped spreading, due to the fact that it becomes less and less likely that an infected person will come into contact with someone who has not had the disease yet (assuming that recovering from COVID-19 confers some immunity). For South Africa this would mean about 48 Million infections in the end.

Now, the great thing about being intelligent beings is that we humans can change our behaviour in response to a disease. We can educate ourselves, share advice, wear masks, wash our hands, stop kissing, practise social distancing and so on. This all has the effect of reducing Rt over time, which reduces the final numbers of infections. The problem is, unless it has eradicated the disease, as soon as a country goes back to "normal", the exponential spread of the disease returns (as in Iran) and we should expect to head towards the relevant herd immunity limit shown in Figure 1.

In the absence of a vaccine, it is hard to keep Rt much lower than R0 for long periods of time since this typically requires severe measures such as lockdown and closing of schools that have dire economic consequences. As a result, unless a country can eliminate the disease relatively quickly - as New Zealand currently appears to have done for example - they must expect a protracted dance with multiple waves of infections.

In South Africa we have so far not been able to achieve and sustain Rt < 1 (like many other developing countries but unlike most 1st world countries). As a result, eradicating the disease will be hard, though we hope not impossible. If we assume we can keep Rt to around 1.5, then we would predict about 60% of South Africa would get infected, i.e. around 36M people.

How many deaths will that cause? Well the Infection Fatality Rate (IFR) is still poorly known. In the early days the best data came from the Chinese CDC which found that about 2.3% of their positive test cases died. This is a worst-case scenario since there are many infections that are missed and not tested. Using the China CDC data leads to predictions for South Africa of about 4800 deaths per 1% of the population infected and hence about 288,000 deaths if 60% of South Africa were infected (Note that because of SA's young population only about 0.8% would die using the Chinese CDC Case Fatality Rates).

Fortunately we now know that the Infection Fatality Rate (IFR) is significantly less than 2.3% in general because of the large number of asymptomatic infections and infections that go undetected due to the limited testing capacity in most countries. Best estimates for the average IFR are now somewhere around 0.3%-1.4% with the lower limit coming from updated numbers from New York City, Madrid and Lombardy. Seroprevalence studies in Spain suggest that about 5.2% of the population have been infected, or about 2.4M people. Given that Spain has had about 27,000 confirmed deaths by mid June, this would put the average Spanish IFR at about 1.1%. Unfortunately this doesn't include missing untested deaths either directly or indirectly due to COVID-19, which could increase the IFR by up to 50%. In South Africa there is no sign yet of excess mortality but there is in the Western Cape.

What should we expect the South African IFR to be on average? There are a number of key points to consider:

1. South Africa's health care system has limited ICU facilities. If you really need ICU care and don't get it, the probability of survival is small. This has already been an issue in hard hit places like Italy, Spain and New York.
2. We have about 8M HIV infections, a high TB burden and a high proportion of hypertension, obesity and

malnutrition. We do not know yet for sure how HIV or the others will affect the IFR for South Africa.

3. South Africa has a young population (only about 5% over 65 years of age) and young people typically have a significantly lower IFR than those over 70.

First world countries have a double advantage over developing countries when it comes to critical care: their lockdowns work more effectively, flattening the curve and reducing pressure on ICU facilities and they typically start with more ICU beds per capita and have greater capabilities to rapidly increase their numbers of ICU beds. South Africa has in the region of 3000-4000 ICU beds including both private and public hospitals. Even the moderate estimates predict peak ICU bed demand exceeding 20,000. Our models predict peak demand could hit 50,000+ which will push up the South African IFR significantly as we discuss later.

Preliminary data from the Western Cape shows that HIV is likely to be a significant factor in South African COVID-19 deaths, with a hazard ratio approximately double that of hypertension, which is a well-known major COVID-19 comorbid condition. For people under 50, HIV was the 2nd most common comorbidity after diabetes. Consider also infant deaths. So far the Western Cape already has 2 younger than five years old, while New York only had 4 deaths under 10 years of age in total out of more than 24,000 deaths.

The bottom line is that we really don't know what the final South African average IFR will be, even if we assume that there is only one important strain of COVID-19, which now looks less and less likely. That means that even if we knew the number of infections perfectly, we are not able to currently predict final deaths to within a factor of 2-3.

So now lets move on to the problem of predicting the final number of infections.

To make precise predictions we need to know our friend Rt for all times over the next year or two. One way to think of Rt is that it is the product of three terms: (1) the probability an infected person will infect someone in a single meeting, (2) the average number of people the infected person meets per day and (3) the number of days they are infectious. And we need to know these three factors for the next 12 months and beyond if we want to predict the total number of infections accurately. A tough ask...

To predict Rt accurately we would need to know what lockdown level the country will be in every month for the next 12 months and also how well the community will comply with the lockdown levels. Just because for example the government mandates a level 5 lockdown doesn't mean people will necessarily comply! Further, we need to know how much of a factor winter will be in the spread of the disease, how many infections we are missing due to limited testing, whether mask usage, contact tracing and quarantining will be effective, and whether there are other, more transmissible strains circulating. We also don't know if blood type will play a role, or whether people will have partial immunity due to previous exposure to the commonly circulating coronaviruses (the non-novel ones). None of these factors are known accurately now. So how should we proceed?

One approach could be to simply take our best guess at what Rt will look like for the next 12 months. That will certainly give us a precise total number of deaths, but should we believe the answer? I could tell you that you have 52,835,834 hairs on your head. That is a very precise answer but it is probably not at all accurate. One way to check is to make lots of reasonable guesses at Rt and see how much our final answers change. If they change a lot we probably shouldn't have much confidence in our guess. So let's do that. A few Rt curves might look like this:

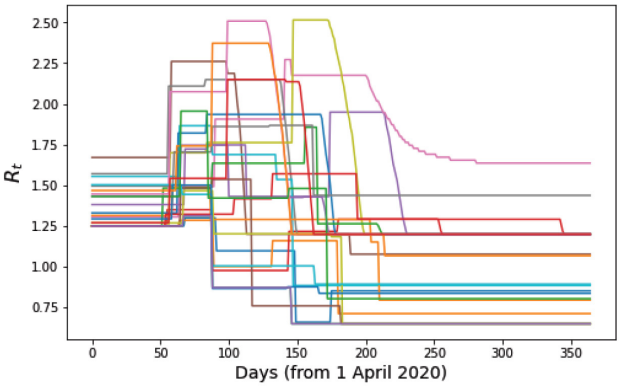


*Figure 2: 25 example curves for the evolution of Rt over the next year*

We choose Rt to start around 1.3-1.6 (since that corresponds to April and May where we have observational data) and then allow it to jump up/down depending on whether one thinks that the lockdown level will go down/up, whether winter will have a big effect or masks will be widely used or be effective etc... Note that when Rt < 1, the daily cases are declining while when Rt > 1 implies that the daily infection numbers will increase (as they have since April to the current date, 12 June). Note that testing plays a crucial role here - if you reduce testing efficiency it may look like Rt < 1 even if, in fact, Rt > 1.

But this small number of scenarios doesn't give us enough feeling for the full range of possible futures. Instead, let's make 2000 such curves. Each one of them represents a possible future, a kind of parallel universe that we might find ourselves in over the next year that is consistent with our current uncertainties about COVID-19, the choices of the South African government and people over the next 12 months, etc...

Then we get something like this:

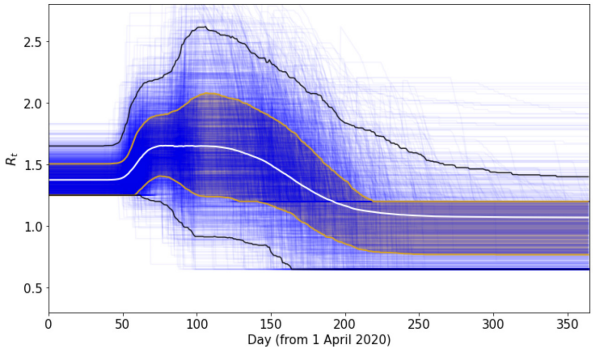


*Figure 3: 2000 simulated Rt curves used for our ensemble over time. They include a death-dependent cutoff on Rt mimicking how people will naturally act in their own best interest as deaths increase, which is why the curves narrow down around 1 over time.*

The white line represents the median value, while the yellow and black lines give the 68% and 95% limits across our 2000 simulations. Note that these 2000 models include a range of pessimistic (Rt > 2), "average" (1 < Rt < 2) and optimistic (Rt < 1) scenarios reflecting the unavoidable uncertainties about the future progression of the disease in South Africa. However, the relative balance between optimistic/average/pessimistic scenarios is not God-given: we still have to make a best guess about the range of possible Rt behaviours that can happen, and this moulds the range of scenarios. As time goes by we will learn whether they were appropriate. That is one of the reasons we have released the code: so you can put in your own beliefs and see what the implications are.

So what do these Rt curves predict? Each one can be run using a compartmental model which follows the flow of people from susceptible through infected and ending either recovered or dead. All the details are available in our report, but the main results are contained in this "horse-tail" plot:

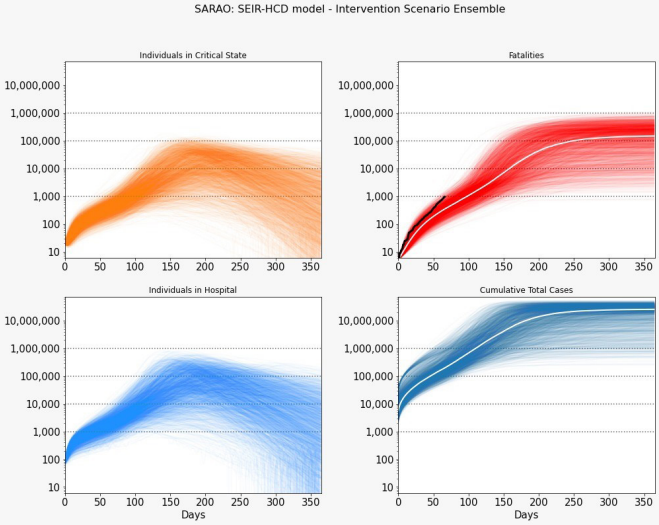


*Figure 4: 2000 simulations starting from 1 April 2020 (day 0) in South Africa and running until the end of March 2021, showing total cases and deaths, and numbers of critical & hospitalised. The white lines represent the median values at each time. The black line in the cumulative deaths (top right) shows the actual South African deaths to June 5. The plots are logarithmic with final deaths (on day 365) running from a few thousand to around 700,000.*

Each panel shows 2000 curves, one for each Rt curve above, starting from 1 April (day 0) and running for 365 days, shown on a log scale.

The important features that you should take away from this plot:

1. There is a huge amount of uncertainty in all quantities: including the final number of deaths, the date and magnitude of the peaks in critical (ICU) and hospitalisation and the total number of infections.
2. Most of our models, starting from 1 April, under predicted the observed deaths in April, May and early June (see the black line in the top right panel). We discuss this more below.
3. The median number of final deaths in our simulations was about 140,000. That means half of our models ended up with more than 140,000 deaths.
4. A significant number of our simulations had a lot of deaths in the first three months of 2021. We must be careful not to let our guard down even if we have a good 2020.
5. Although there were a few percent of simulations with large numbers of deaths (over 400,000) there were also a few percent of simulations with less than 10,000 deaths, representing models in which we are able to bring Rt < 1 and keep it there. The range is very wide.

The latter point is broadly consistent with the CMMID analysis of Low and Middle Income Countries projection of 41,000 to 290,000 deaths in South Africa, though their range is somewhat smaller than ours since their treatment of Rt is significantly simpler.

One critical point, which is actually another manifestation of our main result, is that our range of deaths (from 3,000-700,000), and our median (140,000 deaths), are themselves sensitive to assumptions. Think that we have been too generous on the lower bound of the IFR? Then the lower estimate jumps up. Think that the range of infectiousness period or asymptomatic fraction are wrong? Then the upper bound jumps above 1M or below 400,000. This is all just more grist to the mill of uncertainty: forecasting is hard.

Let's quickly address the issue of why our simulations, starting from 1 April, are mostly under predicting actual South African deaths in April, May and June in Figure 4. Below is the distribution of IFR values in our 2000 simulations both with (red) and without (black) explicit modelling of ICU overwhelm.

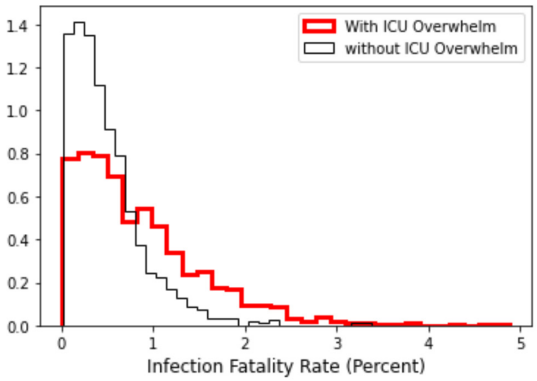


25% of scenarios had an IFR < 0.2% in the no-ICU overwhelm case. Given that HIV appears to be a significant comorbidity for COVID-19 it is likely that this range of IFR values is actually excluded in South Africa. Or it may be a transient effect, driven by our assumptions about Rt which are too tightly constrained at early times, or it may be that we have more undetected cases than our simulations allow for. It is something we will keep track of over the next few weeks, but doesn't affect our main conclusions.

Perhaps you are skeptical about all studies predicting large numbers of deaths or large uncertainties for South Africa? Part of our high numbers are driven by the current uncertainties about the properties of the disease, part by ICU overwhelm (which we discuss below) and part by uncertainties about Rt, as we discussed above. Let's briefly chat about the first issue. There are a lot of parameters that go into making a prediction: a lot have to do with severity: the fraction of asymptomatic patients, the percentage of

patients who will be tested, the percentage of patients who will need hospital treatment etc... But there are other key unknown parameters such as the length of time someone is infectious, which plays a crucial role in determining Rt.

Part of the problem is that available studies are often contradictory, because they are often based on small samples. It is therefore important to allow for the full range of our current uncertainty when making forecasts, not just to cherry pick the results that best fit a particular narrative. For example, some studies assume the asymptomatic fraction to be around 75%. But the comprehensive analysis of the town of Vo' in Italy, where everyone was tested twice, found an asymptomatic fraction around 43%. Assuming 43% for the asymptomatic fraction instead of 75% pushes up predicted deaths significantly. We deal with such uncertainties by also allowing the key parameters to vary within our best estimates of their current uncertainty ranges, but sensible, knowledgable people can disagree on what those ranges are.

It is also critical to appreciate that parameter estimates are often subtly dependent on testing. For example, the fraction of cases needing hospitalisation is often taken to be around 20%, the number found in China. But this fraction is much higher or lower in countries that test less/more per capita than China. In the extreme case, if you only test very severe cases you will, instead, find that nearly 100% need hospitalisation. So if you are in a country that only tests the most severe cases using a 20% hospitalisation fraction will lead to a significant under prediction of deaths.

This is all quite abstract so let's consider a couple of specific toy examples. By "toy" here we mean straw man scenarios that are not realistic models of South Africa but which capture some useful insights. These will provide some intuition about where the high death numbers are coming from.

We will compare four toy scenarios for South African covering two years from April 2020 to March 2022. The first scenario has Rt = 1.05 at all times. This mimics a very strict lockdown that lasts for 2 years. It leads to only about 10,000 deaths, though that number is still increasing after two years as the disease continues to spread slowly through the population. The other three scenarios also all start with Rt = 1.05 but then transition to Rt = 2 after 6, 12 and 18 months respectively. This mimics coming out of lockdown and returning to something like "normal" life. What is notable is that all the three scenarios end up with the same number of deaths: about 470,000, as shown in the Figure 5.

Why doesn't it matter when the lockdown happens in terms of determining the final death toll? Why does't all that hard work for 6, 12 or 18 months count for anything in the end? Well, remember Figure 1? It said that the only thing that mattered in predicting the final infection fraction was the value of Rt. In this case, the most important value was the phase with Rt = 2, which in this toy model case predicts that 80% of South Africa would become infected, and hence that there would be very high numbers of deaths.

Referring to Figure 1 isn't really an explanation of why the long initial lockdown makes no difference though.

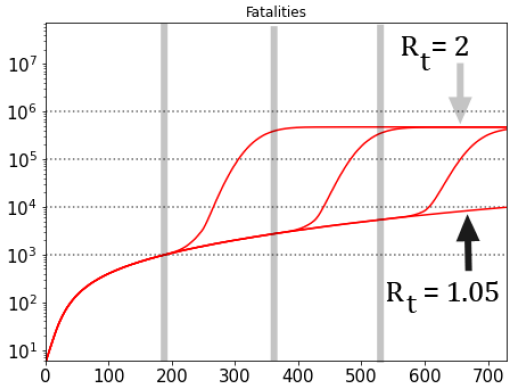


*Figure 5: Deaths over time from 1 April 2020 in four toy scenarios. The first (bottom curve) with Rt = 1.05 for two years, the other three scenarios start with Rt = 1.05 but transition to Rt = 2 after 6, 12 and 18 months (at the grey vertical lines). All of these latter three end with the same number of deaths of about 470,000, independent of when the lockdown ended showing that countries need to be vigilant over long time scales.*

So consider this one instead: COVID-19 may have started spreading in 2019 or perhaps it could have been 2014 or 1998. What matters is when it mutated to become highly transmissible (where Rt is much larger than 1) and that appeared to happen late in 2019. In the same way, it doesn't matter when Rt is small (1.05 in the above scenarios), it only matters when Rt reaches its highest values.

A final analogy might help clarify this important point. Imagine you decide to shoot yourself at midnight tonight but at 11:45 a friend calls you and spends 45 minutes trying to convince you not to. But at 12:30 you hang up and shoot yourself anyway. What did that phone call ("lockdown") buy you? Nothing really - it just delayed the shooting by 30 minutes. In the same way, 18 months of forbearance essentially buys nothing if the lockdown is then released while infections are still spreading. What matters is the maximum value of Rt. If it cannot eradicate the disease then South Africa needs to try to achieve the lowest Rt value that it can afford to sustain over a long period until a vaccine is available. This is not going to be quick, not for South Africa and not for most countries.

An important factor in our pessimistic scenarios where we see a large number of deaths is our modelling of ICU overwhelm; basically demand outstripping supply when it comes to ICU beds. So let's have a brief discussion of what effect South Africa's limited ICU facilities has on fatalities.

**ICU Overwhelm**

South Africa has somewhere in the region of 4000 ICU beds in private and public hospitals. Looking at Figure 4 we see that the peak numbers in critical state (i.e. needing ICU) typically exceed 30,000. At peak only the youngest and healthiest people will be given ICU access. We assume their fatality rate will be around 30% while for the rest their prospects are unfortunately very poor. In Figure 4 we allow it to vary between about 50 and 95% but for concreteness here we assume it is 85%.

To see what effect this has on fatalities let's take our last scenario, the one that starts with Rt = 1.05 and transitions

to Rt = 2 after 180 days, but in the one case we assume everyone has access to an ICU if they need it while in the other only 4000 people have access to ICU at any time. The differences are stark. In the case with no ICU overwhelm only about 210,000 die. When we include ICU overwhelm it rises back to 470,000. Germany's relatively low death rate likely is partly due to their high number of ICU beds per capita relative to Italy, Spain and the UK.

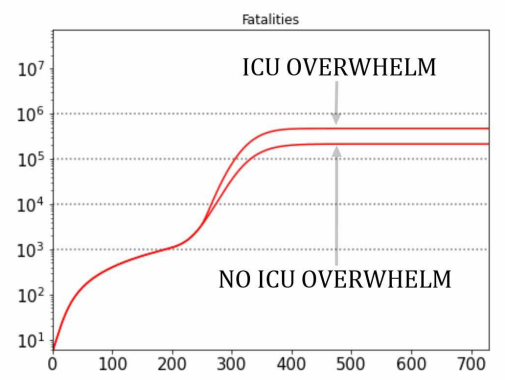


*Figure 6 - In this toy model, ICU overwhelm more than doubles fatalities compared to a model without ICU overwhelm (Rt = 1.05 for 6 months followed by Rt = 2 for the remaining 18 months).*

Unfortunately our conclusion is that ICU overwhelm is likely to significantly increase South Africa's IFR. In Figure 4 it increases the median number of deaths by approximately half. However, the goal of the National Ventilator Project is to reduce the number of people who need ICU.

**The National Ventilator Project**

The National Ventilator Project, managed by SARAO, has the goal of supporting South Africa's COVID-19 response via the large-scale production of non-invasive ventilators. The aim is to reduce the number of people who end up in ICU. We don't yet know how effective this approach will be but let's take our previous toy model and explore the effect of the non-invasive ventilators by assuming they change the fraction of hospitalised patients who end up in ICU in three scenarios: (1) the default value (25%), (2) 17% and (3) 12%. We assume only 4000 ICU beds, so there are extra fatalities from ICU overwhelm.

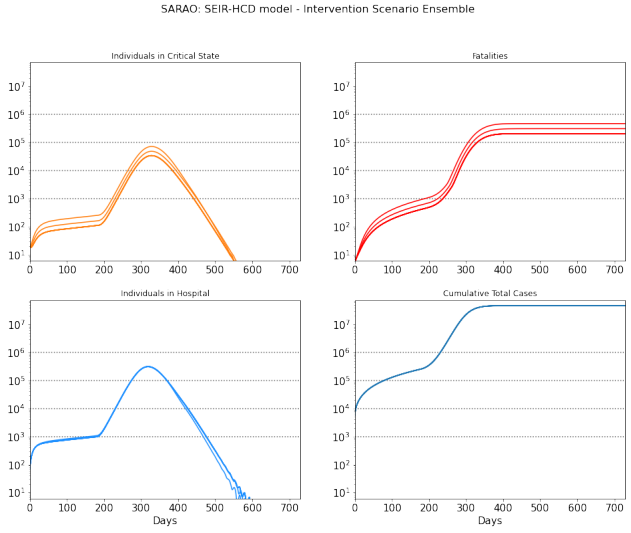


*Figure 7 - the potential effects of non-invasive ventilators on critical cases and fatalities, in our toy model shown on a logarithmic scale. Keeping people out of the critical state is very effective at reducing deaths.*

The results are shown in Figure 7 on a log scale which makes the differences look small but the critical ICU peak for these three toy scenarios changes from 72,000 to 48,000 to 34,000 (top left) which translates into final fatalities of 470,000, 309,000 and 206,000 respectively (top right), showing that investing in non-invasive ventilators may have a massive impact on reducing deaths even in the presence of ICU overwhelm if they can reduce the probability of people transitioning from general wards to high and critical care. Further, such interventions help reduce deaths even in the optimistic scenarios. Note in Figure 7 that there is no change in the total number of cases (bottom right), and only a small change in the number of hospitalised cases (bottom left).

Of course, our toy projections are overly hopeful, even if the non-invasive ventilators are very effective. Figure 4 shows that many of our scenarios have more than 300,000 people requiring hospitalisation at peak. South Africa only has about 100,000 hospital beds (an effect we have not modelled which will further increase fatalities over what we have projected) and even making 50,000 non-invasive ventilators will be a huge undertaking.

**Conclusions**

To summarise our main result: there are scenarios consistent with what we currently know about COVID-19 that have less than 10,000 total deaths, but equally there are scenarios with 400,000 or more total deaths. The future is not yet written: in the absence of vaccine or treatment breakthroughs, what the government and public do over the next 12-18 months will have a huge impact - positive and negative - on the final death toll.

However, the fact that many of our scenarios have high COVID-19 death tolls does not mean we are suggesting that lockdown should necessarily be reimposed or tightened. The hard tradeoffs between COVID deaths, damage to the economy, and the suffering and deaths directly or indirectly caused by strict lockdown are incredibly complex and far beyond the scope of our analysis. But let us not enter into those important discussions with a false sense of security about the worst-case COVID-19 scenarios.

Finally, you might argue that the compartmental models we have used are not sophisticated enough to accurately model the pandemic in South Africa and the world. Absolutely. They are relatively simple models. But more complex and realistic models must out of necessity have many more unknown knobs, levers and parameters that we don't know or can't know yet, and that extra flexibility will lead to even more uncertainties in the long-term pandemic predictions, so going to a more realistic model will not change our main results. It is like accurate long-term weather forecasting: it's just beyond our capabilities currently. For while I may hope that the weather will be 25C and sunny at 10am on 1 December from six months out, but I won't believe anyone who claims they can predict it with any confidence.

Our report with full technical details, and discussion of limitations and next steps, is available at https://docs.google.com/document/d/1WBri6wTXfwqwz4K18Yvt2vRan-ydz18RwgGZJLJHuLg/edit?usp=sharing.

"All models are wrong, but some are useful" - George Box.

# Deep learning holds enormous promise for automating the labelling of bioacoustic data

*Authors: Emmanuel Dufourq, Ian Durbach, James P. Hansford, Amanda Hoepfner, Jessica V. Bryant, Heidi Ma, Christina S. Stender, Samuel T. Turvey*

Deep learning holds enormous promise for automating the labelling of bioacoustic data. The number of applications is growing, but the majority of datasets are still labelled manually, even as the rate of data collection makes this increasingly unsustainable. The mismatch between the potential of deep learning approaches and their actual uptake among practitioners occurs because getting models to perform as well as an experienced human is difficult. Human-like performance usually requires substantial amounts of training data or relatively stable background environments, conditions that are often absent in ecological surveys. Model tuning and data manipulation is often required, and while guidelines are emerging these can, with some justification, appear subjective and case specific. A lack of computing resources and user-friendly software can also be a barrier to entry.

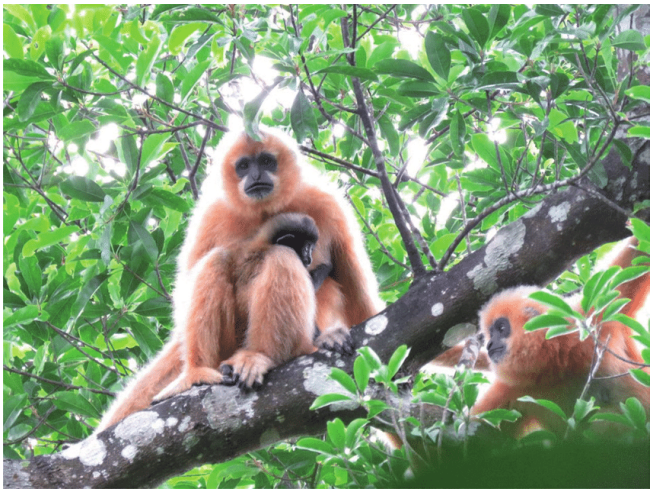

*Hainan gibbon, extracted from Zhou, Jiang and Deng, Huaiqing, Two Endemic Primates' Species in China: Hainan Gibbon and Guizhou Snub-Nosed Monkey. 2019*

30 individuals believed to exist in the wild. The acoustic monitoring project was established in 2015 to better understand gibbon population size and structure, movement patterns, and space use. Passive acoustic recordings were made by a fixed microphone (or array of microphones) located in situ in the gibbons' habitat, and set to record for several hours each day.

Case studies reporting successful applications play an important role in developing and disseminating best practices, and in discriminating between those tasks that current deep learning methods are able to automate and those they cannot. No studies to date have reported the process of applying deep learning at the scale of a typical acoustic monitoring project designed to answer a well-defined research question.

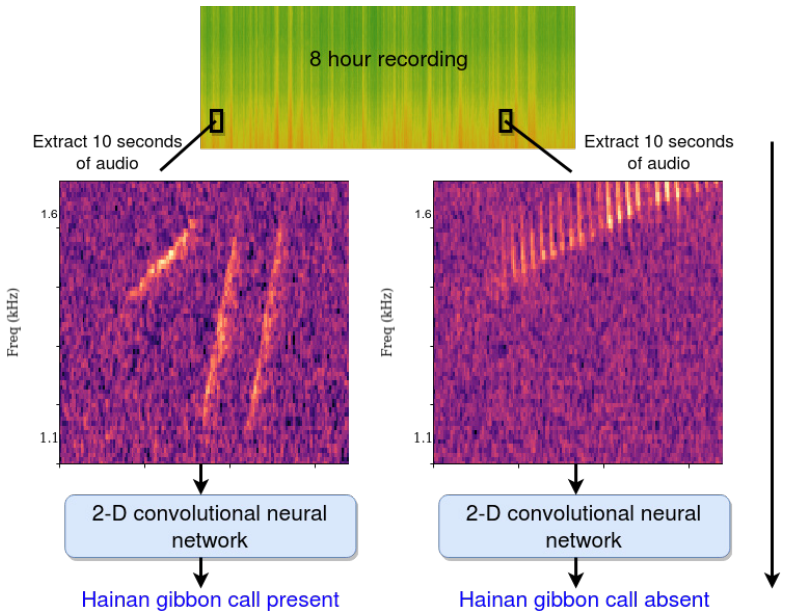


*Illustrating how an 8 hour audio file is processed by extracting 10 second segments and processing it through our 2-D convolutional neural network.*

We explored the development of 1-D (raw amplitude inputs) and 2-D (converted spectrogram input) CNNs. Our 2-D models allow new recordings to be classified on a per-second basis, to a high degree of accuracy. An 8 hour input file can be processed in 6 minutes and on 72 hours of testing data we obtain, on average, 3 minutes of false positives and 38 seconds of false negatives. Despite 3 minutes of false positives, our model will greatly facilitate the process of manually annotating these datasets by ruling out large portions of recordings that have a near-zero probability of containing gibbon song and guide the practitioner to correct areas of large 8 hour files.

Our efforts describe the development of a classifier for identifying Hainan gibbon (Nomascus hainanus) calls in passive acoustic recordings collected as part of a long-term monitoring project whose conditions illustrate both the appeal and difficulty of automation. Hainan gibbons are one of the world's rarest mammal species, with fewer than

# Harman : a normalisation method for genomic data sets

*Authors: Milaine Seneu Tchamga and Gaston K Mazandu*

There are now large-scale data coming from genome projects and generated using multiple time points at various lanoratories by different platforms. Therefore batch effects are now potentially increased. Currently there are multiple batch evalutation and correction methods. These methods sometimes fail to produce all the underlying batch effects. In this article we review Harman and compare it with two other methods ComBat, ExploBatch.

Harman was developed first and foremost, to tackle the double edged problem with batch effects – to optimise batch noise removal with the constraint that the risk of also removing genuine biological variance is quantified andkept to a sensible level determined by the user.

Let us consider the case where the smallest amount that the user is ready to say that there are batch effects in the data set is smaller than the confidence percentage. It follows that the amount of batch mean dispersion comes from the batch noise. Given a principal component (PC) the sample score is given by,

$$c_{kj} = AB_k + s_{kj}, \quad (1)$$

with $i = 1, .., N$ and $k = 1, .., b$, where $c_{jk}$ is the score corresponding to the $j^{th}$ sample in batch $k$ with batch mean $AB_k$ , $N$ the number of samples per batch, and $b$ the number of batches. $s_{kj}$ thus becomes the distance between the sample score $c_{kj}$ and the center of the batch to which it belongs.

Removing the noise or batch effect means as much as possible ”drawing back” or ”reducing” the observed batch mean dispersion under the condition that the limit set by the user is not greater than the confidence value. Put another way, the corrected version of $c_{kj}$ is given by

$$c_{kj}(corrected) = r.AB_k + s_{kj}, \; 0 \leq r \quad (2)$$
$$< 1 \; such \; that \; L(dk(corrected)) = 1 - confidence \; limit \quad (3)$$

where $L$ is the overall probability.

We apply Harman to a dataset with noise. The dataset used was made of 25 genes. We measured the error made and compared it with that of two other methods namely Combat and ExploBatch. We plot the result. See Figure 1. It can be observed that Harman is the one with the least amount of error made. It is therefore the best method.

We can conclude that Harman’s ability to better remove batch noise, and better preserve biologically meaningful signal simultaneously within a single study, and maintain the user-set trade-off between batch noise rejection and signal preservation across different studies makes it an effective alternative method to deal with batch effects in high-throughput genomic datasets. Har-man is flexible in terms of the data types it can process. It is available publically as an R package.

(https://bioconductor.org/packages/release/bioc/html/Harman.html), as well as a compiled Matlab package (http://www.bioinformatics.csiro.au/harman/) which does not require a Matlab license to run.

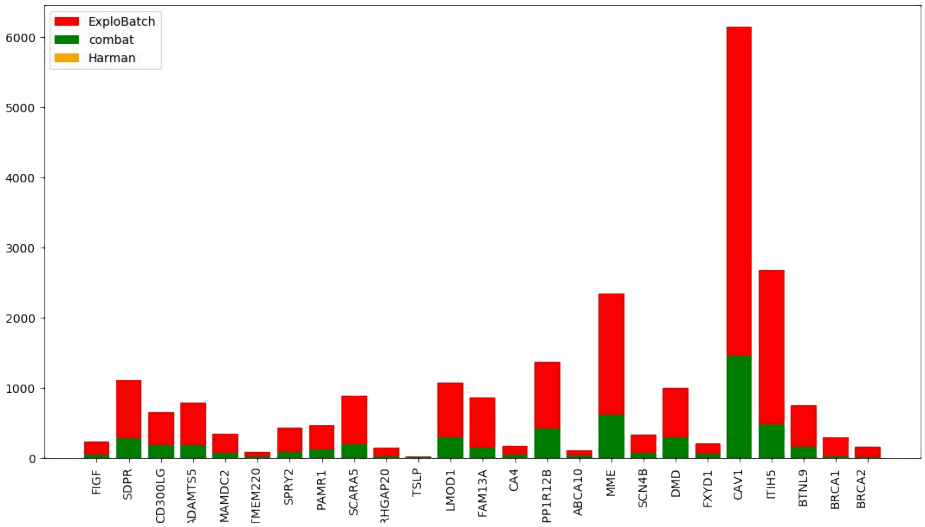


*Figure 1: Result of the sum of error for the three methods: ExploBatch, Combat and Harman*

# Traffic Accident Forecasting using Deep Learning

*Authors: Shankar Agarwal, Bubacarr Bah*

Deep learning has given a huge boost to the rapidly developing field of computer vision. With Convolutional Neural Network (CNN), a range of new applications of computer vision techniques are now becoming part of our everyday lives. These include face recognition+indexing, automation in self-driving vehicles and radio controlled aircraft, medical diagnostics, monitoring the health of crops and livestock, and more. In the past few years, another deep learning algorithm, the Recurrent Neural Network (RNN), has shown an outstanding ability in labelling and prediction tasks for sequential data, such as in financial markets, climate/weather phenomena, and medical events.

According to reports from the World Health Organisation and the South Africa Transport Department approximately 1 million road accidents, with around 14000 deaths, are reported in South Africa, per year. On average over 40 people are fatally injured and over 20 left permanently disabled, daily. Currently in computer vision, anticipating road accidents is much less addressed than anticipating events such as making a turn or changing a lane, since accidents are rare events and usually occur in many different ways, against a backdrop of diverse seeing conditions and background traffic. To overcome these challenges, we aim to combine the power of CNN with RNN to predict the future occurrence of road accidents. The dataset consists of 1750 traffic videos (each video is 4 seconds long and has 100 frames) recorded using dashboard mounted cameras.

For example, in Figure 1 we show 3 frames from an accident video clip, at time -1.56, -0.52 and 0 seconds before the accident. You can see the two motorbikes collide at $t = 0$ seconds. Note that the other 97 frames are not shown for visual clarity. Of the 1750 videos, 620 involve an accident. All accident videos are clipped such that the moment of accident corresponds to $t = 0$ second mark, together with the recording of the accidents from $t = -3.6$ seconds before the accident to $t = 0.4$ seconds after the accident.


*Figure 1: Top row: CNN-predicted Regions of Interest, RoI (in blue) for 3 frames from a traffic video involving an accident at $t = 0$ second mark. Above each RoI is shown its attention value (in red). Higher the attention, the higher the chance that the corresponding RoI could be involved in an accident. RoIs with attention value above 0.4 are plotted in green boxes. The time to accident and the probability of accident are quoted within each frame. Bottom row: RNN is used to predict showing the probability of accident (along y-axis) at each of the 100 frames (each frame is 0.04 seconds long). RNN triggers an alarm if accident probability goes above the trigger threshold of 50% (red dashed line).*

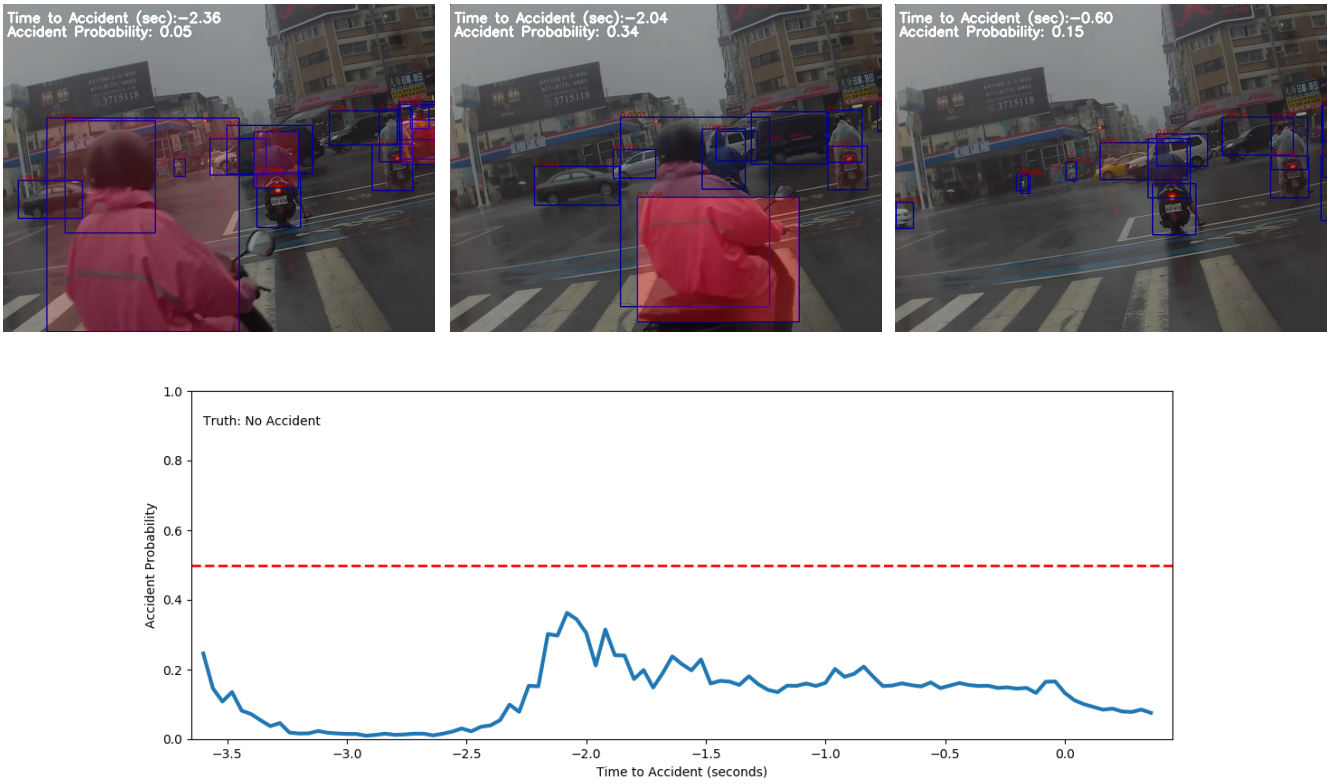


*Figure 2: Similar to Figure 1, but this video clip does not involve any accident. Note that the accident probability stays under the trigger threshold of 50% (red dashed line) throughout the video clip, thus no alarm is triggered by the RNN model at any stage.*

Our accident prediction recipe is as follows: First, we use an object detection code to detect regions of interest (RoI) in each frame of a video clip. In Figure 1, RoIs in a frame are shown in blue boxes. Each RoI is then fed into a state-of-the-art CNN to extract N-dimensional feature representation of the RoI. This N-dimensional encoding tells us what class the RoI belongs to. We track 5 classes: human, bicycle, motorbike, car and bus. These steps are repeated for each of the 100 frames of a video. The N-dimensional feature vectors from each frame essentially form a time-series dataset, which can be fed into a RNN model to anticipate an accident. The RNN is trained to model the temporal relation between video frames. The goal is to then predict, at each frame, whether an accident is imminent. Since accidents are scheduled to happen at $t = 0$ second mark, a well trained RNN should trigger an alarm much earlier than $t = 0$ seconds.

In Figure 1 (bottom row), we plot the probability (along y-axis) of a forthcoming accident for each of the 100 frames (along x-axis, where each frame is 0.04 seconds long) of a video clip. One can see that at $t = -0.52$ seconds before the accident actually happens, the RNN model anticipates an accident to occur with 55% probability, and shortly thereafter the probability of an accident goes up to 100%. If the RNN is set to trigger an alarm at probability 50% (red dashed line), then the driver will be alerted of an imminent accident at about $t = -0.5$ seconds before the accident. This is very encouraging since very often, avoiding accidents is a split second decision. Lowering the trigger threshold to 20% would sound the alarm at about $t = -1$ second mark, thereby giving the driver even longer time to take collision avoidance or mitigation steps.

In Figure 2 we show a video clip that has no accident. It involves a motorbike (in red jacket) coming from behind and riding across the vision of the driver. A well trained RNN should predict "no accident" for this example. In the top row, middle frame, you can see that the accident probability spikes up to 0.34. This is because the RNN anticipates the red motorbike will most likely hit either the motorbike in front, or hit the vehicle recording the video. As the red motorbike steers clear of all traffic, the accident probability drops back down (see plot in bottom row). Setting the RNN trigger probability threshold to 20% would produce a false accident alarm. Thus, setting the RNN trigger to a high value helps to keep the count of false alarms low, but much more importantly, can be detrimental to saving lives. For traffic accidents, the cost of a RNN model missing to report a true accident far exceeds the nuisance of a false alarm, thus it is advisable to have a lower RNN trigger threshold to minimise false negatives. Our RNN model's precision is $\sim 68\%$. In other words, for every 100 traffic videos for which the RNN sounds an alarm $\sim 68$ videos indeed have an accident while $\sim 32$ videos have no accidents and turn out to be false alarms.

This CNN+RNN approach to anticipate accidents can easily be extended to a range of other applications, such as anticipating criminal activity using video recordings from security cameras.

# Random graph ensembles to model equilibration timescales of isolated quantum systems

*Authors: Daniel Nickelsen and Michael Kastner*

Equilibration is a thermodynamic process during which energy is exchanged between a system and its environment, until the system settles into a stationary state – a process ubiquitous in nature and forming the cornerstone of many applied sciences. The justification of equilibration, however, is still resting on the *fundamental assumption* of statistical mechanics, instead of being a rigorous result from first principles. The fundamental assumption states that all microstates that realise a certain macrostate are equally probable.

Thinking of a cup of hot coffee in a room, equilibration would be the process of heat exchange between cup and room until the coffee has cooled down to room temperature. In that example, possible microstates are different sets of positions and velocities of all molecules in the room. In terms of the fundamental assumption, we observe equilibration because the cup-room-system is overwhelmingly more likely to take one of the microstates realising equal temperatures, because this macrostate is realised by overwhelmingly more microstates than other macrostates. If all microstates would not be equally likely, we could have a situation where particular microstates corresponding to hot coffee and cold room are more likely, and we would not observe thermodynamic equilibration.

As quantum mechanics governs the dynamics of microstates, it serves as the first principle in attempts to proof the fundamental assumption. As a linear theory, however, quantum mechanics does not predict single, deterministic trajectories like in classical mechanics, but instead considers all possible linear superpositions of states of the entire system. The probability of finding the system in a certain superposition state is, in general, not uniform and as such contradicts the fundamental assumption. Yet we know from everyday life experience and numerous experiments that the fundamental assumption cannot be entirely wrong.

Recent research has worked out that the theory of quantum mechanics as a basis for realistic models is too general, and certain additional properties have to be imposed to ensure that predictions of quantum models are in line with everyday life experience. A currently debated candidate for such a property is *locality*, which corresponds to the intuition that objects predominantly interact with their local surroundings.

As a new way to incorporate locality into quantum mechanical models, we propose to encode quantum systems as weighted graphs, where the superposition states of the system are encoded as the nodes of the graph, and the weights of the edges are derived from the coefficients of the linear dynamics. It turns out that locality is reflected in three structural properties of these graphs: the sparseness, the degree distribution, and the bandedness, see Figure 1. Generating random graphs respecting these properties constitutes a potential new way to model realistic quantum mechanical models in agreement with the laws of thermodynamics.

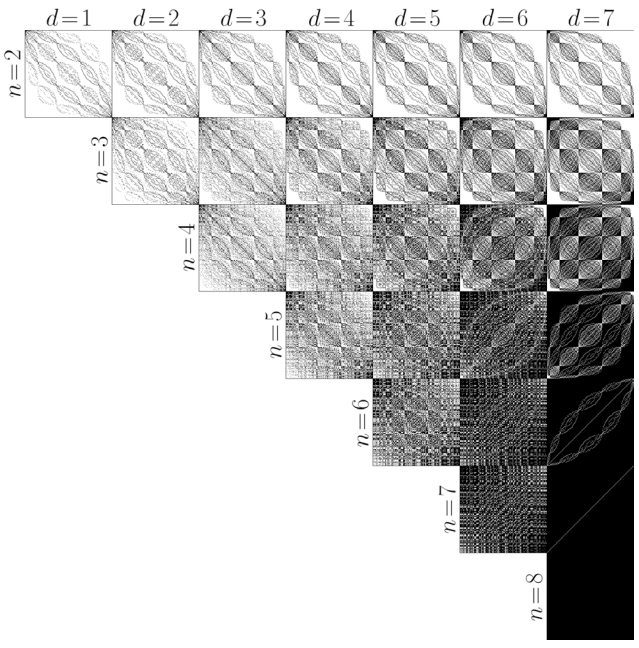


*Figure 1: Adjacency matrices of graphs derived from quantum spin chains with different degrees of locality. The parameter n is the number of spins simultaneously involved in interactions, and d is the maximum distance across which these interactions take place. Strong locality corresponds to n=2 and d=1 (top left), while n=8 and d=7 implies no locality (bottom right). The graphs have 256 nodes, edges are indicated by black pixels.*

A popular benchmark criterion for such an agreement is the prediction of equilibration timescales $T_{eq}$ consistent with thermodynamics which proved to be more realistic using the proposed random graphs compared to alternative random matrix approaches. In addition, the equilibration timescales turned out to be strongly correlated with the maximum flow value $f_{\max}$ of a network defined on the graph, as shown in Figure 2, which allows estimation of equilibration timescales for system sizes otherwise inaccessible.

Apart from deriving the laws of equilibrium thermodynamics from quantum mechanics, it is debated how to even define equilibrium in a quantum mechanical setting. The challenge

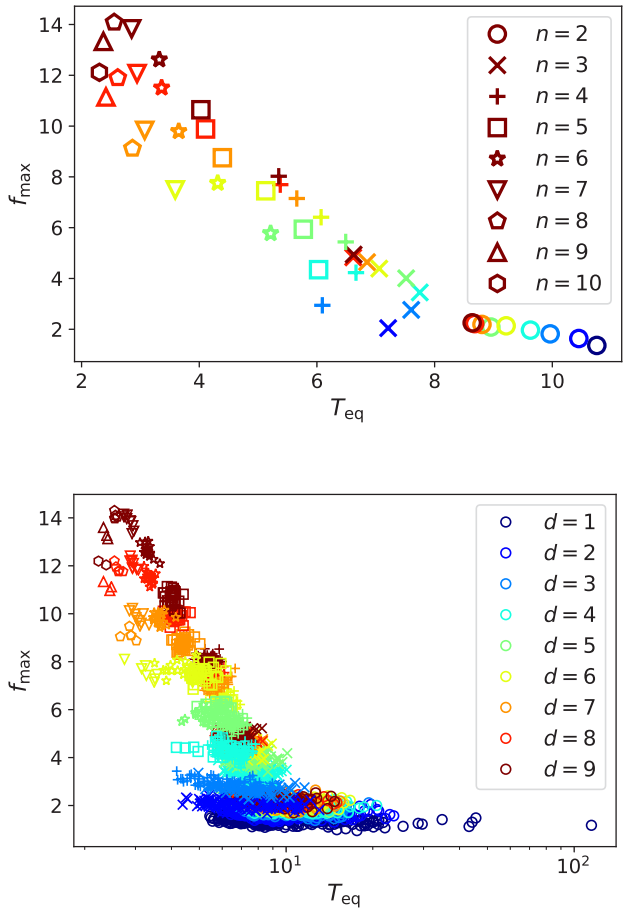


*Figure 2: Maximum flow values $f_{max}$ versus equilibration timescales $T_{eq}$ measured in repeated numerical experiments on the quantum systems that give rise to the graphs shown in Figure 1. The lower plot shows the results of each experiment, the upper plot displays the respective averages for all possible combinations of n and d.*

is that the underlying equation of quantum mechanics, the Schrödinger equation, is time reversal, which is in contradiction to the notion of equilibration. Referring again to the coffee cup example, time reversal would mean that the cooling down of hot coffee as well as the spontaneous heating of the coffee to its initial temperature are both valid solutions of the Schrödinger equation. While we observe the former every day, the latter has presumably never been observed. The key in resolving this paradox is again the notion of probability: it is in fact possible that a cup of cooled down coffee spontaneously heats up again, but with a probability smaller than winning every single gamble happening on earth in one lifespan.

While this probabilistic explanation has already been established in statistical mechanics without reverting to quantum mechanics, it is notoriously dicult to apply this reasoning to quantum mechanical time evolution. To tackle this difficulty, we suggest to rewrite the Schrödinger equation as an extremely high dimensional stochastic process, where the only randomness stems from the preparation of the initial state of the system.

This is a realistic model: while the time evolution is deterministic, the preparation of an initial state intrinsically involves some randomness according to the widely accepted Copenhagen interpretation of quantum mechanics. It appears that the resulting stochastic processes have a family of stationary states in line with other definitions of equilibrium, but potentially offering a more robust and complete description of equilibration with many new lines of further research.

# Deep Learning improves identification of Radio Frequency Interference

*Authors: Alireza Vafaei Sadr, Bruce Bassett, Nadeem Oozeer,Yabebal Fantaye and Chris Finlay*

Radio astronomy observatories are driven to the quietest regions on earth in an attempt to escape the relentless contamination from man-made radio emissions including satellites, television, radio, cell phones and aircraft. Despite this, contamination from Radio Frequency Interference (RFI) is often orders of magnitude stronger than the astronomical signals of interest and hence must be carefully removed from the science data. RFI will increasingly be a limiting factor for high quality science observations with current and planned radio telescopes, such as the MeerKAT, the South African precursor of the Square Kilometer Array (SKA).

There have been numerous techniques devised to address the excision or mitigation of RFI from observed data. Historically approaches have fallen into three broad classes: linear methods, such as Singular Vector Decomposition (SVD) or Principle Component Analysis (PCA); threshold-based algorithms, such as cumsum and SumThreshold, where RFI is flagged when data exceeds some threshold in the smoothed 2D time-frequency plane; and finally Supervised Machine Learning, where the algorithm learns from examples of RFI classified by expert astronomers. Deep learning that has been used on simulated single dish data with a U-Net architecture delivered  better results, as measured by the Area Under the ROC Curve (AUC) and precision-recall metrics, compared to SumThreshold methods.

Our work extends this result by exploring new deep architectures and, in particular, now demonstrates superiority on simulated interferometric data sets using our new RFI simulator for telescope arrays.

We use a a Convolutional Neural network (CNN) based model, is inspired by the residual network architecture ResNet (that we call R-Net) to do a binary classification of every pixel of the time-frequency images given the pixel and those around it. The data used consisted of; HIDE is a simulated single dish visibilities, MeerKAT which consist of 64 antennas interferometric simulation and KAT-7 which is a real visibility observation that has been flagged by astronomers. The output is a binary mask image of the same size. R-Net is very simple in terms of its architecture (Figure. 1) since it consists only of convolutional layers with zero paddings to save the size through layers. After each convolutional layer (except the last one) we insert a batch normalization and RELU activation layer. The hyperparameters of such an architecture are the number of layers, kernel size, number of filters, location of shortcut(s) and activation function.  Searching the hyperparameter space is very time consuming and limited by available computing resources: our exploration of the potential hyperparameters was guided by intuition and trial and error applied to the validation set.

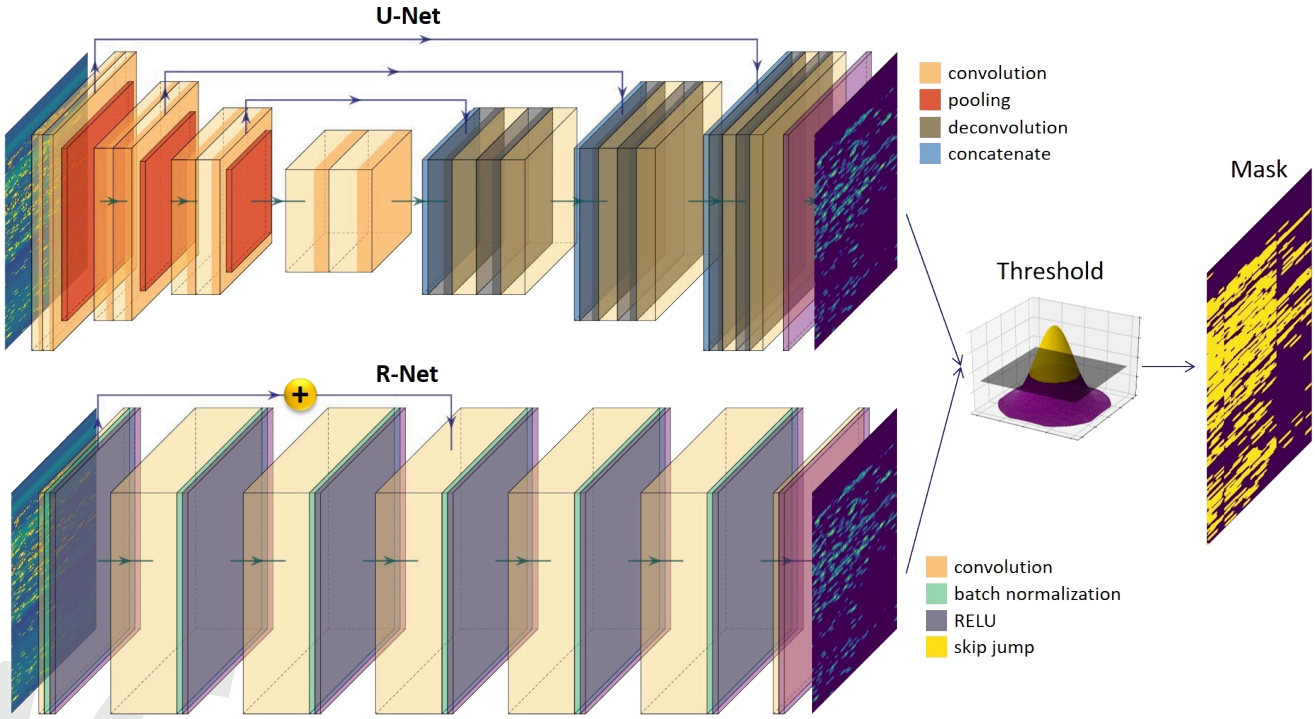


*Figure 1: Schematic views of the U-Net architecture (top) and our new R-Net algorithm (bottom). Both algorithms predict RFI probabilities for each pixel in the map. The final binary mask is produced by passing the output maps through a thresholding process which is one of the hyperparameters for the algorithms.*

All of the hidden layers in the R-net contain 12 filters and the kernel size is always 5 x 5. R-Net does not change the input size through layers so any number of hidden layers works; we try 3, 5, 6 and 7 numbers of layers. A shortcut (residual network) connection directly transfers information from earlier layers to the deeper layers to avoid the degradation problem. We used no shortcut connections for the 3 layer architecture, one for the 5 and 6 layers architectures and 2 shortcut connections for the 7 layer architecture. Our initial results show the performance of the 5 and 6 layers architectures (hereafter R-Net5 and R-Net6) provide the best performance in terms of AUC.

To compare R-Net against the other two reference algorithms (U-Net and SDP-Flagger*) we consider several metrics, in particular the area under the True Positive Rate (TPR)-False Positive Rate (FPR) curve and the AUC. Since the datasets we considered can be significantly unbalanced, the Precision-Recall curve, F1-score and Matthew correlation coefficient (MCC) are calculated as well for each case. We found that the 5 and 6-layer versions of R-Net outperform all other variants of U-Net and SDPFlagger significantly in all metrics, as shown in Figure 2.

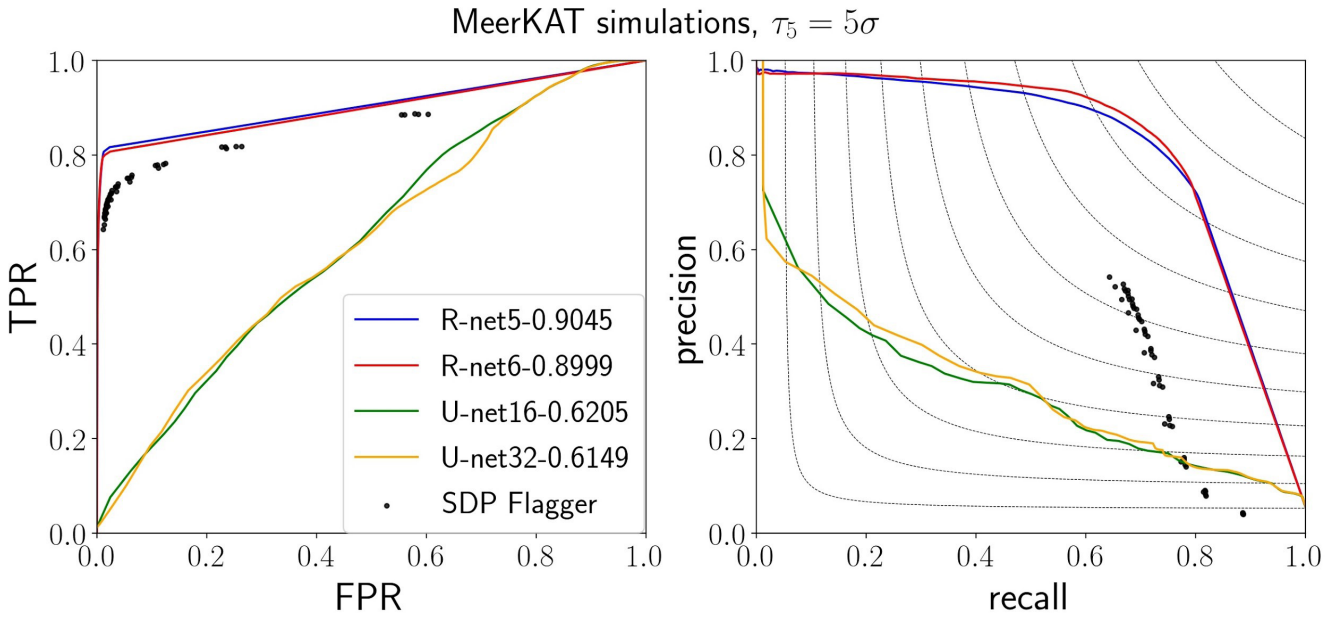


*Figure 2: R-Net significantly outperforms both U-Net and the SDP Flagger trained on MeerKAT simulations using only the absolute value of the visibility data (RFI threshold of 5). The legend shows corresponding AUC values for R-Net and U-Net. Note the significant drop in performance of all algorithms relative to their corresponding results on the much simpler HIDE data. Dots show the SDP Flagger results using different hyper parameters. Although the SDPFlagger does relatively well on the TPR-FPR curve it performs poorly for all values on the precision-recall plot. Contours denote iso-F1 scores. For all datasets used in our analysis, we varied the SDP Flagger hyperparameters, outlier-n-sigma (O) and background reject (Rb). The results are shown as the point cloud.*

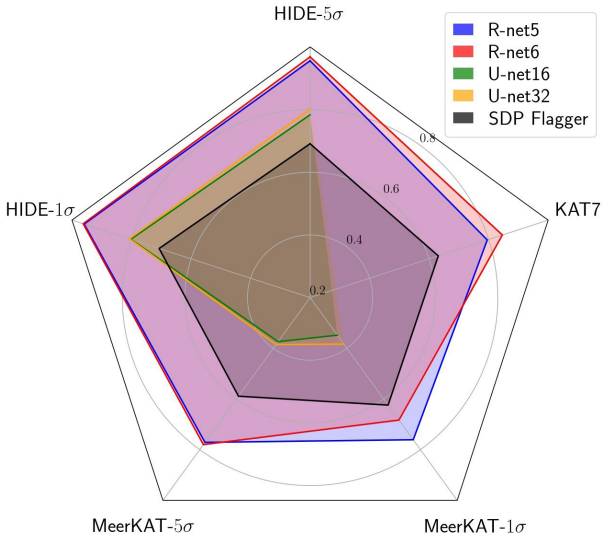


*Figure 3: Star plot comparison between F1 scores of all the algorithms for all the datasets and different thresholds (e.g. HIDE-5 corresponds to the results where the threshold is 5). The center corresponds to a score of zero and the outer contour to a perfect score of 1. R-Net outperforms all other algorithm variants as it encloses all other algorithms on all datasets and thresholds. Note that U-Net was not included for the transfer learning task on the KAT-7 dataset.*

We further highlight the effectiveness of transfer learning from a model initially trained on simulated MeerKAT data and fine-tuned on real, human-flagged, KAT-7 data. Despite the wide differences in the nature of the two telescope arrays the model achieves an AUC of 0.91, while the best model without transfer learning only reaches an AUC of 0.67.

A summary of the performance of all the algorithms on all the datasets and all thresholds is shown in Figure 3.

In conclusion we describe a new ResNet-style convolutional neural network algorithm (R-Net) for Radio Frequency Interference (RFI) flagging. We have tested this algorithm on both single-dish and realistic interferometric telescope array RFI simulations showing that it significantly outperforms the current state-of-the-art algorithms including both U-Net and the modified version of AOFlagger currently used in the MeerKAT data reduction pipeline.

* SDP Flagger is the SARAO Science Data processing in-house RFI flagger, which is based on the known AOFlagger by Ofringa (2017)

# Assessment of model risk due to the use of an inappropriate parameter estimator

*Authors: Modisane B. Seitshiro and Hopolang P. Mashele*

**Introduction**

During the financial crisis and its systems reformation that took place in the years 2007 to 2009, financial risk prediction was identified as a major concern for the public afterwards. As a result, an understanding of model risk, especially the parameter estimation risk for predictive models is now a significant interest to academics, policy makers and practitioners. According to Tunaru (2015), parameter estimation risk is a problem in that the dynamic model's specification and parameter set are viewed as being known by the financial model developers and users whereas the true parameter values are basically not known with certainty.

In the literature, we compare several statistical methods and unconstraint optimization methods for obtaining the minimum cost function from the binary LRM, which is an objective model that has not been looked at for different organizational fields and academic problems (Minka, 2003; Diers, Eling and Linde, 2013; Borowicz and Norman, 2006; Millar, 2011). Yang, Brown, Moran, Wang, Pan and Qin (2016) show the use of Iteratively Reweighted Least Squares (IRLS) and Kalman Filter with Expectation Maximization (EM) in measurement error covariance estimation. They reveal that on average the IRLS converges quickly and gives a more accurate parameter estimate for the model of interest, which was backed by the work of Diers et al. (2013). Dinse (2011) adopted the EM method for fitting a four-parameter LRM to binary response data, and confirms that EM method automatically satisfies certain constraints, such as finding variance-covariance matrix of estimates, that are more complicated to implement with other parameter estimation methods. Hinton, Sabour and Frosst (2018) achieved significantly better accuracy when using EM algorithm. Stochastic Gradient Descent (SGD) and its variants were versatile parameter estimators that have been proven invaluable as learning algorithms or step size for large datasets (Bottou, 2012). Advice from the Bottou (2012), is for a successful application of these Batch Gradient Descent (BGD), Mini-Batch GD (MBGD) and SGD to be considered when one performs small-scale problems, whereas the majority of researchers allude that the methods work efficiently for large-scale problems (Robles, Bielza, Larrañaga, González and Ohno-Machado, 2008; Ruder, 2016). Conjugate Gradient (CG) method was applied for comparison of three Artificial Neural Network (ANN) methods in the application of bankruptcy prediction (Charalambous, Charitou and Kaourou, 2000). The line search Newton CG methods such as Truncated Newton (TN) method have been highly effective approaches for large-scale unconstrained optimization (Dembo and Steihaug, 1983), but their use for LRM has not been fully exploited, hence it has been considered in this article. Some of the most popular updates for minimizing the cost function of binary LRM, are the Broyden, Fetcher, Goldfarb and Shanno (BFGS) method and its variant Limited-Memory BFGS (LM-BFGS) methods. The LM-BFGS is mostly used to save on the memory needed for computation of the Hessian matrix that BFGS method usualy waste (Nocedal and Wright, 2006). The Nelder Mead (NM) simplex method developed after the Powell's (PW) method is considered to be performing efficiently for the computation of symmetrical balanced binary response in a widely used LRM (Noubiap and Seidel, 2000; Powell, 1964).

The contribution of this article is presenting different parameter estimation methods for predicting PD through binary LRM and determining optimum parameters that minimize the objective model's cost function. The parameter estimation method with a minimum cost function among the other methods is considered to be the better parameter estimator. Thus, the high the binary LRM cost function the more inappropriate the parameter estimator becomes.

**Parameter estimation methods for predictive models**

In this section, the binary LRM with its cost function using eleven parameter estimation methods are briefly described. In order to examine factors influencing a decision of whether an obligor experiences a default event or not, we consider the following binary LRM to quantify the PD model, recommended by Neter, Kutner, Nachtsheim and Wasserman (1996):

$$Y_i = \mathrm{X}_{i,p}^T \boldsymbol{\gamma} + \varepsilon_i \tag{1}$$

where $Y_i$ is a binary response variable indicating the status of the obligor, which should satisfying the following:

$$Y_i = \begin{cases} 1; \text{ if default event occurs} \\ 0; \text{ otherwise} \end{cases}$$

$\mathrm{X}_{i,p}$ is the design matrix of $p = 2$ predictor variables with the sample size $n \in \mathbb{N}$, cases $i = 1, 2, \ldots, n$, $\boldsymbol{\gamma}$ is the vector of parameters for the binary LRM and assume that the error terms $\varepsilon_i$ are independent and identically logistic distributed. We let the conditional probability $\pi_i = P(Y_i = 1 \mid \mathrm{X}_{i,p}^T)$ to be PD event given the predictor variables, denoted by the logistic function as

$$\pi_i = \frac{1}{1 + e^{(-\mathrm{X}_{i,p}^T \boldsymbol{\gamma})}}. \tag{2}$$

Therefore, the estimator of interest is shown as

$$\hat{\boldsymbol{\gamma}} = \arg\max_{\boldsymbol{\gamma}} [\mathscr{L}(\boldsymbol{\gamma})] = \arg\min_{\boldsymbol{\gamma}} [\mathscr{C}(\boldsymbol{\gamma})], \tag{3}$$

To find the estimates given in equation (3), we use the different estimation methods. The BGD method is a first-order iterative optimization algorithm for finding the minimum of a nonlinear function. It minimizes the cost function iteratively by starting from an initial random value and update the parameter values using some step size referred to as the learning rate. The SGD method is an alternative and simplified version of the BGD for minimizing the differentiable cost function. The MBGD is a sub-method of the BGD and SGD that partition the dataset into small batches of dataset, used to compute the model cost function. The sum of the gradient over the mini-batch reduces the time spent for approximated convergence and the average of the gradient further reduces the variance of the SGD. The IRLS is a numerical method used to find the optimum parameter value. It is one of the fastest and most applicable methods

for minimizing a cost function is the NR method. Utilizing the first-order Taylor series approximation and determining the starting estimate, usually through the Ordinary Least Squares (OLS). The EM method may be utilized to obtain the maximum log-likelihood expectation for the parameter of interest. Here, we utilize the method for minimizing the cost function. The NM simplex method has always been the most widely used method for nonlinear unconstrained optimization. The PW method is an optimization method that approximates the minimum value of a function by making an assumption that the partial derivatives of the cost function does not exist. The CG is a method that efficiently avoids the calculation of the inverse Hessian by iteratively descending on the conjugate directions. The TN method is also known as the inline search Newton CG method and use predictable amount of computational storage. The BFGS method is a Quasi-Newton method also known as a variable metric algorithm. This is a nonlinear optimization method for solving unconstrained problems. The LM-BFGS method is an extension of BFGS method that belongs to the variants of Quasi-Newton optimization problems. For model risk mitigation the optimal parameter estimation method should ensure that the cost function is minimized among all other optimization method.

## Results

In the effort of trying to address Model Risk with respect to parameter estimations risk, we compare the performance of the parameter estimates when the binary LRM is applied to estimate the PD. All **t**he codes of the analysis were computed on Python version 3.7.1 with Jupyter Notebook version 5.7.4.

We set the parameter intercept $\gamma_0 = 0.0$ and the parameter slope $\gamma_1 = 0.5$. Therefore, we use the simulation to produce the balanced dataset of default and non-default events. For each of true parameters and sample size of 6 400, the dataset was simulated and analyzed. To keep our model simple, we included only one predictor variable which is uniformly distributed (i.e., $X_i \sim U[-8;8]$) for which the cost function $\mathscr{C}(\boldsymbol{\gamma})$ is investigated. The dataset was simulated using the LRM and setting the parameter to 0.5 for a Bernoulli distribution resulting in a dichotomous response variable $Y_i$ indicating whether an event occurred or not. The PD is then estimated through the use of LRM given in equation (2).

We use the accuracy rate $\mathscr{A}$ to assess the performance of the optimized parameters in the accuracy model given in equation (2), which is expressed as

$$\mathscr{A} = \frac{\sum_{i=1}^{n} [I(\hat{\pi}_i \geq 0.5) \equiv (Y_i = 1)] + \sum_{i=1}^{n} [I(\pi_i < 0.5) \equiv (Y_i = 0)]}{n},$$

where $I(.) = \{0;1\}$ is the indicator function and $n$ the sample size.

## Applications to real dataset

This section is based on the application of the proposed methodology in section 2 to the benchmarking dataset. The anonymous dataset collected during the years 2016 to 2018 is from one of the South African financial institutions that provide loans to clients. The dataset contains the history of 1057 clients with the default indicator been the binary response variable ($Y$), i.e. default = 1 and non-default = 0. To empirically compare the simulation and the real data results, we only considered one predictor variable ($X_i$). This variable is the average percentage credit to disposable income of the clients recorded monthly over the given period. Tables 1 and 2 presents the results of the optimized parameters for the binary LRM that minimizes the cost function, computed using 11 different parameter estimation methods. The BGD method described was configured to run 100 iteration for the simulated dataset but reveals convergence of the cost function $\mathscr{C}(\boldsymbol{\gamma})$= 0:3881 in only two iterations (i.e. $\kappa = 2$).

**Table 1:** Parameter estimation method results for PD using Binary LRM

| *Parameter estimator* | $\mathscr{I}$ | $b$ | $\kappa(\varepsilon)$ | $\hat{\gamma}_0$ | $\hat{\gamma}_1$ | $\mathscr{A}$ | $\mathscr{C}(\boldsymbol{\gamma})$ |
|---|---|---|---|---|---|---|---|
| **BGD** | 100 | 1 | 2(0.01) | 0.0051 | 0.4914 | 0.8294 | 0.3881 |
| **SGD** | 100 | 1 | 10(0.01) | 0.0075 | 0.4898 | 0.8294 | 0.3881 |
| **MBGD** | 100 | 1 | 10(0.01) | 0.0099 | 0.4996 | 0.8292 | 0.2936 |
| **IRLS** | 100 | 1 | 7(1e-08) | 0.0134 | 0.4930 | 0.8291 | 0.3881 |
| **EM** | 100 | 1 | 39 (1e-08) | 0.0134 | 0.4930 | 0.8291 | 0.3881 |
| **NM** | 100 | 1 | 88 (1e-08) | 0.0239 | 0.4977 | 0.8236 | 0.3853 |
| **PW** | 100 | 1 | 2 (1e-08) | 0.0239 | 0.4977 | 0.8236 | 0.3853 |
| **CG** | 100 | 1 | 9 (1e-08) | 0.0239 | 0.4977 | 0.8236 | 0.3853 |
| **TN** | 100 | 1 | 8 (1e-08) | 0.0239 | 0.4977 | 0.8236 | 0.3853 |
| **BFGS** | 100 | 1 | 10 (1e-08) | 0.0239 | 0.4977 | 0.8236 | 0.3853 |
| **LM-BFGS** | 100 | 1 | 9 (1e-08) | 0.0239 | 0.4977 | 0.8236 | 0.3853 |

Notes: The $\mathscr{I}$ is iterations, $b$ is the random mini-batch size, $\kappa$ is convergence of iterations and $\varepsilon$ is the tolerance level in brackets, $\mathscr{A}$ is the accuracy level. $\mathscr{C}(\gamma)$ is the cost function. *NB* for MBGD 40 sub-batches were generated from the sample size.

**Table 2:** Parameter estimation method results for PD using Binary LRM on real dataset

| *Parameter estimator* | $\mathscr{I}$ | $b$ | $\kappa(\varepsilon)$ | $\hat{\gamma}_0$ | $\hat{\gamma}_1$ | $\mathscr{A}$ | $\mathscr{C}(\boldsymbol{\gamma})$ |
|---|---|---|---|---|---|---|---|
| **BGD** | 100 | 1 | 10(0.01) | 0.1426 | 0.0883 | 0.6244 | 1.3172 |
| **SGD** | 100 | 1 | 10(0.01) | 2.1909 | 0.1115 | 0.6244 | 2.3416 |
| **MBGD** | 100 | 1 | 10(0.01) | 0.2211 | 0.1369 | 0.6244 | 0.2564 |
| **IRLS** | 100 | 1 | 4 (1e-08) | 1.1281 | -0.0179 | 0.6339 | 0.6559 |
| **EM** | 100 | 1 | 8 (1e-08) | 1.1281 | -0.0179 | 0.6339 | 0.6559 |
| **NM** | 100 | 1 | 85 (1e-08) | 1.1281 | -0.0179 | 0.6339 | 0.6559 |
| **PW** | 100 | 1 | 60 (1e-08) | 1.1281 | -0.0179 | 0.6339 | 0.6559 |
| **CG** | 100 | 1 | 14 (1e-08) | 1.1281 | -0.0179 | 0.6339 | 0.6559 |
| **TN** | 100 | 1 | 15 (1e-08) | 1.1281 | -0.0179 | 0.6339 | 0.6559 |
| **BFGS** | 100 | 1 | 8 (1e-08) | 1.1281 | -0.0179 | 0.6339 | 0.6559 |
| **LM-BFGS** | 100 | 1 | 17 (1e-08) | 1.1281 | -0.0178 | 0.6339 | 0.6559 |

Notes: For MBGD 12 sub-batches were generated from the sample size.

## Conclusion

In Section 2, the binary LRM is proposed as a default model to assess model risk with respect to parameter estimation risk, that is inappropriate parameter estimation method. The paper recommended numerical optimization methods as parameter estimators for estimating the model parameters through minimization of the binary LRM cost function. It is revealed that parameter risk is important and essential through the comparison of numerical experiments and simulation done in section 3. MBGD method is shown to outperform the alternative optimization methods. MBGD estimators are accurate, since the bias is smaller among alternative methods, i.e.

$$E(\hat{\gamma}_1) - \gamma_1 = 0.4996 - 0.5 = -0.0004$$

Disregarding parameter risk can lead to a significant under-estimation of risk capital requirements, depending on the size of the underlying datasets. Therefore, we conclude that predicting PD using the binary LRM with the known varying thresholds will lead to substantially different results when parameter risk is taken into consideration. That is, when several optimization methods are employed. Numerical optimization estimation methods are identified as been the ones that have parameters which minimizes the cost function or maximizes the log-likelihood function of the simple binary LRM. The impact of parameter estimation risk is depicted for an optimization method that yield the lowest cost function. Our experimental results support the need for further research of estimation parameter risk for binary LRM and other family of exponential models. Binary LRM with high order of predictor variables and interaction terms with different distributions may exhibit high parameter estimation risk implications. Therefore, it can be explored for further research of parameter estimation risk. Model risk management researchers and practitioners are therefore encouraged to consider parameter estimation risk through exploring different optimization methods as opposed to using the same traditional estimation methods repeatedly.



https://www.cogentoa.com/article/10.1080/23322039.2019.1710970.

# A Robot Glossary

*Author: Simukai W. Utete*

To be able to navigate the world, a robot requires capabilities beyond navigation. Intelligent autonomous systems must be able to make sense of a world populated with people, where scenes are dynamic and in which reasoning, and meta-reasoning, may be called for. This is the setting of interest – the field – and field robotics provides a rich, diverse set of challenges, interesting in themselves, and with diverse application.The navigating robot requires a range of capabilities, and an ability to unify them, as a task demands.

**Data Fusion**

One of the fundamental capabilities a robot might have is the ability to fuse data. For example, in mobile robotics, a vehicle might make use of camera, laser, sonar and other data types. Data fusion is the combination of data to form a picture of an environment, and is fundamental to robotics. It is also applicable to numerous other domains where data from diverse sources must be combined, for example. in environmental monitoring.

Decentralised data fusion systems, and decentralised systems in general, involve the processing of data over a distributed system, of sensor nodes, for example, but also across robots or other agents (see Further Reading). Decentralised systems are of particular interest because of their power and applicability in different problem settings.

Alongside fusion is the idea of breaking things into shares and how this could be done. First, why would this be done? In spread spectrum systems, a signal can be spread for transmission over a channel, to be reconstructed at the receiver, as in radar signal processing or in the Aloha communications system, of which more later. This process has multiple uses. Intelligent sensor networks and robots can benefit from being able to fuse diverse data and to break data into shares.

**Coordination**

People are good at coming up with solutions in action, online, as information changes. One capability important in software engineering and for computer systems is graceful degradation. In systems of multiple robots, there can be rules for interaction. If a set of rules fails, it is important that a system can respond.

In some systems, when a traffic light fails, the control of traffic moves to use of a four-way stop. This is an example of graceful degradation, and of central control transferring to coordination by local agents. As a coordination mechanism, it has a number of important properties. For example, the four-way stop method could be considered as achieving fairness (at some cost in terms of efficiency). A driverless car could be programmed to understand that this is the rule that applies; it could even learn from observations that this is the case. More interesting still would be groups of cars that are able to coordinate to achieve a similar outcome.

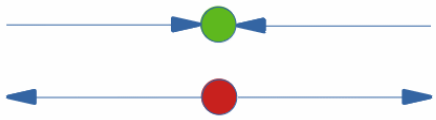

In many problems, it is beneficial to be able to achieve a global outcome from local interactions, for example in decentralised interactions. In the literature, Pearl identifies a number of conditions for a form of distributed control system. As noted by Pearl (see Further Reading, below), meeting the conditions, as does an edge reversal algorithm of Gafni and Bertsekas, amongst other algorithms, solves a form of the dining philosophers problem. In the edge reversal algorithm described in the reading, a directed acyclic graph (DAG) is imposed on a network of nodes. Nodes consider the edges incident on them, Sinks (like the green node, above) are considered to fire or to be on. On firing, the edges change direction, and the new sinks fire and so on. A number of distributed problems fall into the class of problems noted by Pearl, which are amenable to solution by edge reversal.

With edge reversal, local interactions lead to a type of global solution. A four-way stop (or n-way stop) is an instance of a problem potentially amenable to solution by edge reversal. Edge-reversal control could identify the allowed travel across an intersection, in an efficient manner, with a lane needing to consider only a local signal. In this way, multiple junctions could also be chained together, with precedence controlled via the local interactions along edges, once the original DAG has been imposed, since edge-reversal provides a form of distributed turn taking.

In fact, a traffic light can be considered a means of coordination by Aumann's correlated equilibrium (Rescoria 2019). Coordination can also be achieved by convention (Rescoria 2019). There is an extensive literature on both areas. Convention can be used to resolve coordination problems, so driverless cars and autonomous agents in the field must know or determine the applicable conventions. An interesting idea is the norm of coordination for these autonomous agents – whether and how they can determine their own conventions and what those would be.

There is an extensive literature on coordination games, and coordination in the face of multiple equilibria can be solved by reference to convention, amongst other means. (In fact, in the literature, a traffic light is seen by some as an example of coordination using Aumann's concept of a correlated equilibrium; see Further Reading, for an article on convention and its use in coordination.) Driverless cars and highly autonomous systems in the field must know or determine the applicable conventions. An interesting idea for these autonomous agents is whether and how they can determine their own conventions and what those would be.

Interoperability is another potential concern for driverless cars, distributed devices or other autonomous agents seeking to coordinate. Some aspects of interoperability involve the problem of handling multiple equilibria. The agents must also make group decisions, for example via voting. Another consideration is that events considered rare might not be so in a fully autonomous situation, where many autonomous agents work together, driven by processing on numerous devices of similar type.

**Active Problems**

Many problems fall into this category, including active vision problems. Put simply, an active problem concerns a situation where there is a limit on position such that a restricted set of viewpoints must be used to solve the problem. This is central to the problem of adaptive sampling, in robotics and in other applications. In active sensing, viewpoints might be restricted because of occlusion or because it is feasible to sample only a limited number of points. But active problems arise in time too, in condition monitoring, environmental monitoring and even situational assessment (needed by the navigating robot); a potential event must be detected via precursor samples in time before it occurs.

**Games and Meta-reasoning**

A capability that is useful for an autonomous system is the ability to reason about the reasoning of other agents. Common knowledge problems are ubiquitous in distributed systems. The navigating agent must also to be able to recognise the way that games and mechanisms work. Game theory and the theory of combinatorial games offer tools useful for achieving systems with high levels of autonomy. The driverless cars at the failed traffic light could reason via games to a four-way stop mechanism, a mechanism that allows each one a turn. In combinatorial games, position can be important. The outcome of the game might have been determined from the first position of play, or there might be a means of winning via strategy stealing. A robot able to recognise the game structure in an interaction could exploit this for its own or its group's advantage.

**Synthesis**

Biomimetic algorithms are of interest in many areas, for example in radar, or for the development of other types of sensor (see Readings for an example of bat-inspired sonar for mobile robotics applications). Animals such as bats can communicate in clutter, managing collisions in sound, yet still able to use echolocation to detect objects. The way that they behave in groups and the systems they form are particularly interesting for robotics applications.

The Aloha system mentioned earlier was developed by Abramson and a group at the University of Hawaii, in the 1960s (see Further Reading for a history of the Aloha system). Some communications and biological researchers have likened aspects of Aloha processing to bat communication. In the pure Aloha algorithm, processors communicate asynchronously along a shared channel. This means that collisions can occur. On collision, the processors wait a random time before attempting to transmit once more.

In a game structure, one could consider two robots, A and B, communicating using a frequency channel, so sharing spectrum and represent this situation, with payoffs to be applied, as:

| A/B | f1 | f2 |
|---|---|---|
| f1 | collide | transmit |
| f2 | transmit | collide |

If the robots signal using the same frequency in close proximity, there is a collision. If spatial placement allowed for their organisation in a network with links between immediate neighbours they could use the edge reversal mechanism seen earlier to take turns signalling.

In nature, in some cases, collision leads to bats going to a higher frequency. (This is a simplification. The range of behaviours of bats and their calls are complex and nuanced.) In radar, this higher frequency is useful as pulses could then be separated and the channel shared in a manner akin to forms of software-defined radio and other similar systems. A robot able to learn to do this would be starting its own form of coordination. Auctions are a mechanism that is often applied to share spectrum. The collision avoidance chirps are like bids, a way to share spectrum in a physical system.

**Anti-Patterns**

In operating systems and software development, there are anti-patterns, patterns that should not arise. One can consider what the uses of these might be in a similar way to the discipline of stochastic resonance, a field that investigates uses of noise. Mechanisms can be undermined by behaviour outside the intended scope; for example, bidding rings or other forms of collusion would be a problem for auctions. An interesting example of collusion (allowed) is seen in an international Iterated Prisoner's Dilemma competition which allowed multiple entries per team and was won by colluding agents (see Further Reading). Here collusion could be seen as a form of anti-pattern cooperation.

Consider again in this light the two robots sharing a frequency channel. As mentioned, in the pure Aloha algorithm, devices communicating along a common channel, could communicate asynchronously, with collisions allowed. On collision, the processors waited a random time, then re-transmitted. Now consider robot 'bats', able to share a communication channel and change frequency. If they transmit on the same frequency, a collision occurs, the interaction above. Their next interaction could be represented as below.

If they go up in frequency, they now find that their discrimination is higher, a new game ensues, where they have shared the channel, by raising their bid. But they would have taken the first move in another game, made a bid and found a way to cooperate and made a first move towards interoperability. They have also created shares. Many methods make use of the partitioning space at finer resolution, for example, occupancy grids applied in the robotics literature or adaptive sampling at different scales

in robotics and other domains. The readings include some examples of these. Going up in frequency means the robots are operating at a higher resolution. Taken as a whole, a system of this type is a new type of transmitter. (Although of course there are more complexities to the behaviour of groups of bats and communicating processors.)

| A/B | f1 | f2 |
|---|---|---|
| f1 | game2 | transmit |
| f2 | transmit | game2 |

So far, only a single further move has been considered, not the possibilities and limitations of further moves, including the point at which further moves are not possible (i.e. what is the form of game2?). The limits of a game must be known. A game paradox is presented by Zwicker, in the form of a game, Zwicker's Hypergame, where a move in the game is the selection of a particular type of game, of which the game could be one (a paradox of self-reference, see Readings).

For the transmitting robots, the skill which is sought is the ability to put capabilities together and synthesise something. The navigating robot aims to do something new. Somehow the robot recognises what needs to be done and acts in new and innovative ways. It would need not only to be able to step outside interaction structures via meta-reasoning but to develop new forms of interaction. With the ubiquity of distributed devices, in a range of domains, these issues are of wider application than field robotics.

**Further Reading**


M. Schwartz and N. Abramson, "The Alohanet - surfing for wireless data [History of Communications]," in *IEEE Communications Magazine,* vol. 47, no. 12, pp. 21-25, Dec. 2009, doi: 10.1109/MCOM.2009.5350363.

Bolander, Thomas, "Self-Reference", *The Stanford Encyclopedia of Philosophy* (Fall 2017 Edition), Edward N. Zalta (ed.), URL = <https://plato.stanford.edu/archives/fall2017/entries/self-reference/>.

Hugh Durrant-Whyte, A Beginners Guide to Decentralised Data Fusion, Technical Report, Australian Centre for Field Robotics, The University of Sydney, 20 July 2000.

D. S. Jacobs, *Evolution's chimera: Bats and the marvel of evolutionary adaptation.* UCT Press, Cape Town, 2016.

Jenna Jarvis, William Jackson and Michael Smotherman. Groups of bats improve sonar efficiency through mutual suppression of pulse emissions, *Frontiers in Physiology,* Vol. 4, 2013. URL=https://www.frontiersin.org/article/10.3389/fphys.2013.00140 (accessed 16 July 2020)

R. Kuc and B. Barshan, "Bat-like sonar for guiding mobile robots," in *IEEE Control Systems Magazine*, vol. 12, no. 4, pp. 4-12, Aug. 1992

SY Chong, J. Humble, G. Kendall, J. Li and X. Yao, The Iterated Prisoner's Dilemma: 20 Years On, Chapter 1, in A*dvances in Natural Computation – Volume 4*. The Iterated Prisoner's Dilemma, 20 Years On, G. Kendall, X. Yao, SY Chong (Eds), World Scientific, 2007.

N Govender, J Claassens, F Nicolls, J Warrell, Active object recognition using vocabulary trees, IEEE Workshop on Robot Vision (WORV), 2013.

Naomi Ehrich Leonard, Derek Paley, Francois Lekien, Rodolphe Sepulchre, David M. Fratantoni and Russ Davis, Collective Motion, Sensor Networks and Ocean Sampling, *Proceedings of the IEEE*, Vol 95, No. 1, pp. 48-74, 2007

Judea Pearl, *Probabilistic Reasoning in Intelligent Systems,* Morgan Kaufmann, 1988.

Rescorla, Michael, "Convention", *The Stanford Encyclopedia of Philosophy* (Summer 2019 Edition), Edward N. Zalta (ed.), URL = <https://plato.stanford.edu/archives/sum2019/entries/convention/>.

Roland Siegwart, Illah R. Nourbakhsh, and Davide Scaramuzza. Introduction to *Autonomous Mobile Robots* (2nd. ed.). The MIT Press, 2011.

William S. Zwicker (1987) Playing Games with Games: the Hypergame Paradox, *The American Mathematical Monthly,* 94:6, 507-514.


# Mathematical approach to the dynamics of tropical cyclones


*Author: Marc Sedjro*


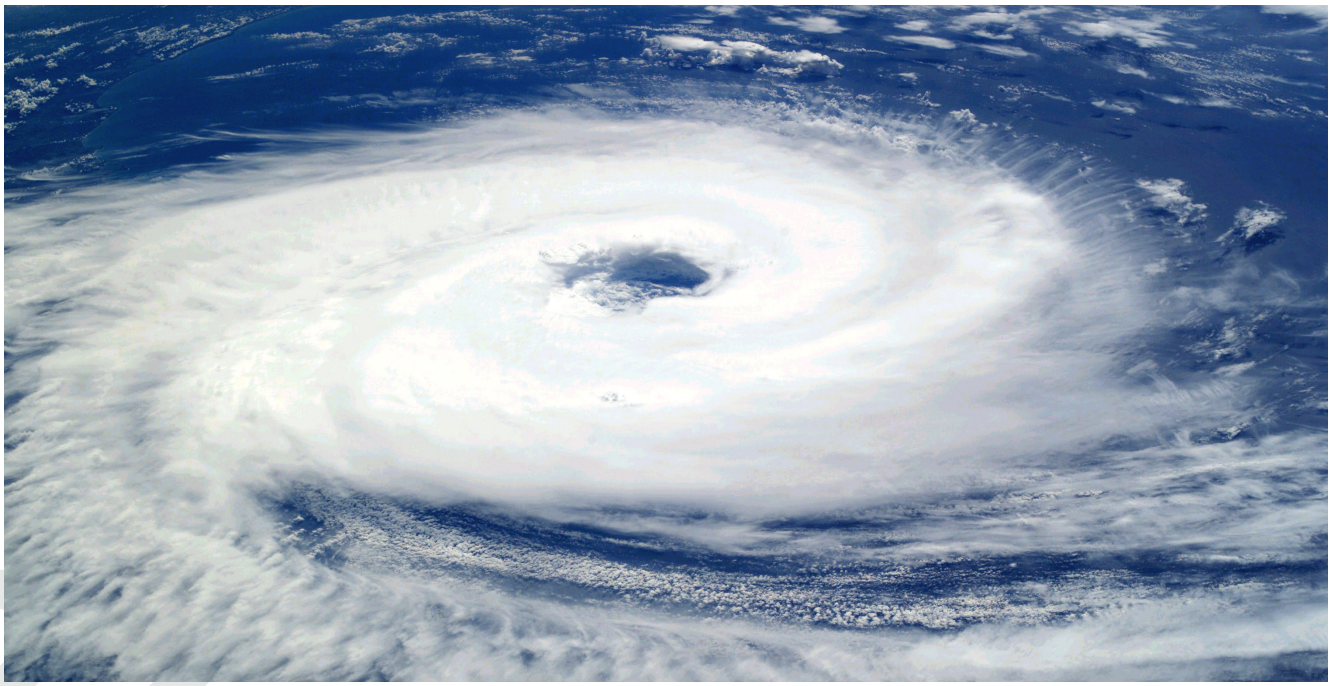

*Figure 1: Tropical cyclone Catarina.*

Tropical cyclones are weather phenomena characterized by a low-pressure center and an intense rotating system of clouds that takes its origin over the oceans. These phenomena occur periodically at various points in the region of the globe situated near the equator between the tropic of Cancer and the tropic of Capricorn. Typically, tropical cyclones are accompanied by heavy rains and strong wind that sadly often have devastating effects on life, infrastructure, and the economy.

From a physical point of view, the study of the dynamics of tropical cyclones falls within the realm of vortex motions. In 1992, George Craig derived a set of equations that are designed to model the dynamics of such vortices in light of fundamental laws of Physics and Thermodynamics. This model was further improved by Michael Cullen who proposed a more realistic framework in which the vortex lies within an ambient fluid at rest with the interface a priori undetermined.

In general, cyclone-like vortices are not easily tractable. However, one can use axisymmetric flows to approximate models of vortices such as the ones introduced by Cullen. In the literature, these flows provide an idealized form of the so-called primary circulations:

$$\frac{u^2}{r} + 2\Omega u = \frac{\partial \varphi}{\partial r} \quad \text{and} \quad g\frac{\theta}{\theta_0} = \frac{\partial \varphi}{\partial z} \ \text{ on } D_\xi \tag{1}$$

Here, $\theta$ denotes the temperature inside the vortex while $\theta_0$ is the ambient temperature out the vorted assumed to be constant and $g$ is the gravity. The equations above are considered on a free boundary domain representing the vortex:

$$D_\xi = \{(r, z): 0 \le z \le 1,\ 1 \le r \le \xi(z)\} \tag{2}$$

where the free boundary is described by a function $\xi$. Additionally, the pressure $\varphi$ is required to vanish on the free boundary of $D_\xi$. To ensure the stability of the vortex one imposes the condition that a variant of the pressure term, namely $\varphi(r, z)+\Omega^2 r^2/2$, is strictly convex. The primary circulation helps understand fundamental structures of tropical cyclones and describes the rotational component of these vortices, which involves the angular velocity $u$ and the Coriolis parameter $\Omega$. The quantities $\theta$, $u$, $\varphi$ and $\xi$ *form the unknowns of the problem in (1) and (2).* We are interested in the question of existence and regularity of a stable solution. In the set of transformed variables $2x_1 = 1 - 2r^{-2}$ and $x_2 = z$, we set,

$$P(x_1, x_2) = \varphi(r, z) + \frac{\Omega^2 r^2}{2} \text{ and } \quad 2b(x_2) = 1 - 2/\xi^2(z) \tag{3}$$

Assuming enough regularity, it turns out that the problem of existence of stable axisymmetric flows can be formulated as a free boundary Monge-Ampere equation of the form

$$\begin{cases} \sigma(\nabla P(x_1, x_2)) \det(\nabla^2 P(x_1, x_2)) = e(x_1) \quad (x_1, x_2) \in \Lambda_b \\ \nabla P(\Lambda_b) = \Sigma \\ P(b(x_2), x_2) = f(b(x_2)) \ \text{ on } \ \{b > 0\} \end{cases} \tag{4}$$

where $f(x_1) = \Omega^2/2(1 - 2x_1)$, and the density functions $\sigma$ and $e(x_1)=1/(1 - 2x_1)^2$ satisfy the compatibility condition

$$\int_\Sigma \sigma(y)dy = \int_{\Lambda_b} e(x_1)dx_1\,dx_2,$$

with $\Sigma$ a bounded set, $\Lambda_b = \{(x_1, x_2) : 0 \le x_1 \le 1,\ 1 \le x_2 \le b(x_1)\}$ and $b < 1/2$. The system of equations (4) is said to have a weak solution in the sense of Brenier if $\nabla P \# e\chi_{\Lambda_b} = \sigma$ holds, along with the third condition of (4). The condition $\nabla P \# e\chi_{\Lambda_b} = \sigma$ means that

$$\int_\Sigma F(y)\sigma(y)dy = \int_{\Lambda_b} F(\nabla P(x_1, x_2))\, e(x_1)dx_1\,dx_2, \quad \text{for all } F \in L^1(\sigma).$$

Although Monge-Ampere equations have been extensively studied, the novelty of problems (4) lies in the treatment of the free boundary of $\Lambda_b$. To examine the existence and regularity of solutions for the class of Monge-Ampere equations aforementioned, we resort to the theory of optimal transport where the total energy of the vortex can be expressed as

$$\sup_{(P,\Psi)} \int_\Sigma \Psi(y)\sigma(y)\mathrm{d}y + \inf_{b\in\mathcal{H}_0} \int_0^1 \int_0^{b(x_2)} (f(x_1) - P(x_1, x_2))\, e(x_1)dx_1\,dx_2. \tag{5}$$

The supremum is taken over the set $\mathcal{C}$ consisting of all continuous functions $(P,\Psi)$ satisfying $P(x) + \Psi(y) \ge \langle x, y \rangle$ and $\mathcal{H}_0$ is the set of Borel functions $b : [0,1] \longrightarrow [0,1/2)$. The problem (5) has a maximiser $(P_0,\Psi_0) \in \mathcal{C}$ where $P_0, \Psi_0$ are Legendre transform of each other and the minimizer $b_0 \in \mathcal{H}_0$ bounded away from 1/2 in the second term of the functional in (5). If $\mathrm{spt}\sigma \subset \mathbb{R}_+ \times \mathbb{R}_+$ then the Euler-Lagrange equation of (5) at $(P_0,\Psi_0)$ yields that

$$\nabla P \# e\chi_{\Lambda_b} = \sigma \tag{6}$$

and

$$b_0(x_2) \in \mathrm{Arg}\min_{0\le\varrho<1} \int_0^{\varrho} (f(x_1) - P(x_1, x_2))\, e(x_1)dx_1$$

whenever $b_0(x_2) > )$ for $x_2 \in [0,1]$. It follows that $(P_0, \Psi_0, b_0)$ solves (4) in the sense of Brenier. Furthermore, the boundary $\partial\Lambda_{b_0}$ is continuous and there exists dual $\lambda > 0$ such that $\lambda \le e \le 1/\lambda$ on $\Lambda_{b0}$. The question of the regularity of the solution and its dual Legendre transform is important for further understanding of the dynamics of tropical cyclones.

To address the regularity issue, we assume that $\mathrm{spt}\sigma \subset \Sigma$ and that $\lambda \le \sigma \le 1/\lambda$ on $\Sigma$. If $\Sigma$ is assumed convex that $P_0$ is strictly convex and the regularity theory developed by Caffarelli ensures that $P_0$ is $C^{1,\alpha}_{loc}$. In the absence of convexity of the domain $\Sigma$, we rely on the theory developed by Figalli. In that case, we strengthen the assumption on the domain $\Sigma$ by requiring that the boundary $\partial\Sigma$ is continuous. Then, there exist two open sets $\tilde{\Sigma} \subset \Sigma$ and $\tilde{\Lambda} \subset \Lambda_{b_0}$ with $\mathscr{L}^2(\Sigma \setminus \tilde{\Sigma}) = \mathscr{L}^2(\Lambda_b \setminus \tilde{\Lambda}) = 0$ such that $P_0 \in C^1(\tilde{\Lambda})$, $\nabla P_0$ is a homeomorphism between $\tilde{\Lambda}$ and $\tilde{\Sigma}$, and

$$\begin{cases} \lambda^2 \le \det(\nabla^2 P_0) \le \frac{1}{\lambda^2} & \text{on } \tilde{\Lambda} \\ P_0(b_0(x_2), x_2 = f(b_0(x_2)) & \text{on } \{b_0 > 0\} \end{cases} \tag{7}$$

in the sense of the Alexandrov.

# Distributing private information

*Authors: Martha N Kamkuemah and Rojo F Randrianomentsoa*

As users of the web we are reliant on distributed systems and take for granted their advantage over the centralised systems we learn to program at AIMS: their eciency due to concurrency, shared resources and lack of a central bottleneck; their fault tolerance due to robustness against failednodes; but their lack of authoritarianism and openness towards location, implementation, interfaces and scalability.

However with that latitude distributed systems have to overcome the difficulties of privacy, security, accountability and so on. In this paper we report work concerning privacy in networks (a) composed of devices with limited computing power (the internet of things), and (b) in a distributed auction.

Our theory unfolds at the level of system design and so applies to any particular implementation. A system is specified in terms of its behaviour from input and state before, to output and state after. We extend that by exploiting epistemic logic to express who knows what when.

**Epistemic logic**
As usual, standard logic is extended with a modal operator $K_A$ for each agent $A$ so that $K_A\varphi$ means agent A knows property $\varphi$. Epistemic logic is distinguished from a logic of belief by knowing only valid properties:

$$\text{if } K_A\varphi \text{ then } \vdash \varphi\,. \tag{1}$$

Fundamental properties of the modal operator also include its closure under logical consequence

$$\text{if } K_A\varphi \text{ and } \vdash (\varphi \Rightarrow \psi) \text{ then } K_A\psi \tag{2}$$

and under conjunction

$$\text{if } K_A\varphi \text{ and } K_A\psi \text{ then } K_A(\varphi \wedge \psi)\,. \tag{3}$$

If the predicate is simply the value of a variable, we say that the agent knows that variable: $K_A x$ means that for some value $t$, $K_A(x = t)$.

A predicate $\varphi$ is *common knowledge*, $C\varphi$, means that each agent knows $\varphi$, each agent knows that each agent knows $\varphi$ and so on.

Here is an example which demonstrates the importance and style of epistemic reasoning in a distributed system simplified by having synchronous fault-free communications.

**The clever princess**
In a kingdom ruled by an evil king his beautiful and clever daughter has come of age. Her suitors come from far and wide to undergo the canonical trials for her hand: slaying dragons, rescuing damsels, etc. One suitor, a well-connected but not very bright prince, has the support of the king.
Finally the suitors have been reduced to a small number for the deciding trial which of course includes the king's favourite, but also a candidate who has won favour with the princess for his shrewdness and commitment to befriending dragons. After consulting with his advisors the king suggests to his daughter a protocol for the final trial, which he assures her will put his favourite at a disadvantage and so should be acceptable to her.

He suggests to her that his favourite stand in the centre of the hall facing the throne. Behind him stands the next candidate, the third behind him and so on in a line, so that each candidate can see only those in front of him. The king proposes to tell the candidates that he is about to put a coronet on each, starting from the rear, which is either gold or silver, at least one of which is gold. The first to shout out correctly the colour of his own coronet wins it and the princess. He tells his daughter that he will in fact put a gold coronet on each.

Naturally the candidates are keen but honest, so shout out if and only if they identify their coronet. The king elaborates to his daughter that his own favourite would see none of the others and so must be at a disadvantage. Does she welcome his suggested protocol?

The princess reflects for a minute, imagining the situation of just three candidates. The front candidate could reason that if his coronet were silver, then the candidate directly behind him would reason that if his were silver then the third candidate would see two silver coronets and be able to identify his as gold. When no identification is forthcoming the front candidate knows his assumption that his coronet is silver must be wrong, and so is able to identify it correctly as gold. Moreover he is the only one able to do so because even after the front candidate identifies his coronet, there are situations in which the others could be either gold or silver.

Used to dealing with her father, the clever princess replies that she welcomes his protocol but sees no reason to put one candidate at a 'disadvantage'. Why not arrange them in a circle, so that each can see the others? Since that is

symmetrical all have an equal chance. Naturally she thinks to herself that the quickest has an advantage, by reasoning as she has just done.

Outmanoeuvred, the king agrees. We leave its conclusion to the reader.

**Proof**
In reasoning about what an agent knows in a distributed system, care must be taken to use global information only if it is available to that agent. In this case, communication is synchronous: by word of mouth or by sight. When the king announces to the assembled contestants that all coronets are gold or silver and at least one is gold, that becomes common knowledge.

Assuming the contestants in the final trial are $i : [1, n]$, and the variable $c_i : \{g, s\}$ represents the type of $i$'s coronet, $g$ for gold and $s$ for silver,

$$C\,(\forall\, i \cdot c_i \in \{g, s\} \wedge \exists\, j \cdot c_j = g)\,. \tag{4}$$

Each contestant knows the linear configuration, and each observes the coronets in front of it but not the others:

$$C\,(\forall\, i \cdot (\forall\, j < i \cdot K_i\, c_j\,) \wedge (\forall\, j \geq i \cdot \neg K_i\, c_j))\,. \tag{5}$$

When a contestant identifies his coronet he shouts out loud and so that fact becomes common knowledge

$$\forall\, i \cdot K_i\, c_i \Rightarrow C\,(K_i\, c_i)\,. \tag{6}$$

That models the system epistemically. Now, what about the princess's argument? And why is it necessary for (4) to be common knowledge when each candidate knows that there is at least one gold coronet by sight?

From (4) and (5) candidate 1 knows

$$K_1(c_1{=}s \Rightarrow K_2(c_2{=}s \Rightarrow \cdots \Rightarrow (K_n\, c_n\,)) \cdots)\,.$$

He then reasons (taking propositional reasoning, like contrapositive, for granted), by (4) and since $K_1K_2 \cdots (\neg \mathrm{K}_n\, c_n)$ by (6), using (2)

$$K_1(c_1{=}s \Rightarrow K_2(c_2{=}s \Rightarrow\ \cdots \Rightarrow (K_{n-1}c_{n-1}) \cdots))$$

where again the last implicand turns out to be false. Iterating, eventually

$$K_1 c_1$$

from which it follows that the first candidate identifies his coronet correctly by (2) and (1).

Furthermore examples consistent with the model show that any other candidate could have either kind of coronet.

To answer our question, Agent 1 has relied on the common knowledge in (4) to depth $n$, Agent 2 has relied on it to depth $n{-}1$ and so on, far more than the depth 1 resulting from each's observation.

**Security of IoT**
In realistic networks communication is asynchronous, error prone and beset by eavesdroppers. So authenticating one's correspondent for a private conversation is a fundamental difficulty, specially when agreement is required on secret encryption keys. We say that agents $i$ and $j$ are authenticated (for a given conversation) iff each is certain of the identity of the other. That may be achieved, in a distributed setting, by exploiting the uniqueness of (public, private) key pairs (to within acceptably high probability as usual) to sign a nonce $n_{i,j}$ so that

$$Auth(i, j\,) := \exists\, n_{i,j} \cdot (K_i\, K_j\, n_{i,j}\,) \wedge (K_j\, K_i\, n_{i,j}) \wedge (K_k\, n_{i,j} \Rightarrow k = i, j\,)\,.$$

In long-range wide-area networks (LoRaWAN) composed of devices like sensors, computation and so use of public key encryption is limited. In addition to authentication (you want to ensure noone else's phone can unlock your garage) a fresh key is used to encrypt each message, and both recipients have to know which key to expect, but if an eavesdropper is able to discover a key $key_t$ at used at session $t$, they must not be able to calculate previous or future keys, so-called *forward* and *future* secrecy:

$$\neg(\forall\, k \neq i, j \cdot K_k\, key_t \Rightarrow \forall\, u \neq t \cdot K_k\, key_u\,)\,.$$

The first author has proved that the LoRaWAN protocol achieves authentication but not forward or future secrecy, and has suggested appropriate modifications.

**Auctions**
In a *sealed bid* auction, bidders submit sealed bids to the auctioneer who compares them and announces the winner (after resolving any ties, which we overlook here). That can be distributed by each bidder broadcasting a commit to a bid which acts as the sealed bid and, when the auction closes, broadcasting a matching *reveal*, from which all bidders can evaluate the winner by comparison, without the need for a central process.

Bidder $i$'s commit consists of the bid $d_i$ hashed with a one-way function $h_i$ which achieves

$$C\,(\forall\, j\ \neq i \cdot K_j\, h_i\,(d_i\,) \wedge \neg K_j\, d_i\,)\,.$$

After $i$ reveals $d_i$ *and* $h_i$, each bidder is able to confirm that the reveal matches the commit in which case

$$C\,(\forall\, i, j \cdot K_j\, d_i\,)$$

and all bidders decide the winner consistently.

Distributed auctions and their dominant strategies have been studied by the second author.

**Acknowledgements**
The authors thank their supervisor, Prof. J W Sanders, for his support and the coordination of this article.

# Research Centre Contributors

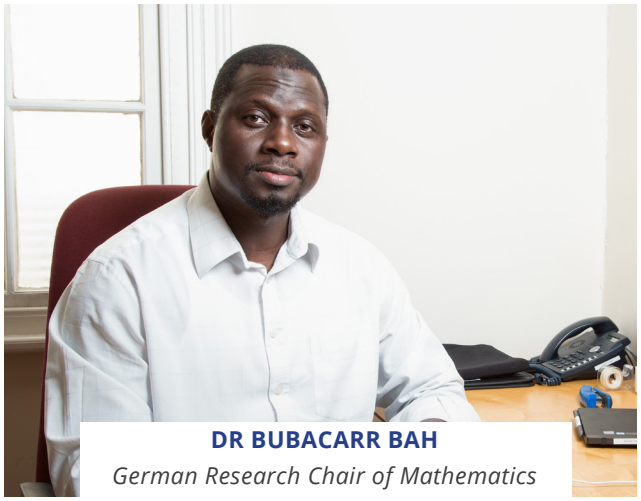

**DR BUBACARR BAH**
*German Research Chair of Mathematics with specialization in Data Science*

**PROF. BRUCE BASSETT**
*Senior Resident Researcher, Head of the Cosmology Group*

**PROF HOPOLANG PHILLIP MASHELE**
*Part-time Senior Resident Researcher Financial Mathematics*

**DR GASTON K MAZANDU**
*Part-time Researcher AIMS-H3ABioNet*

**DR MARC SEDJRO**
*German Research Chair for Applied Mathematics with specialization in Partial Differential Equations and Calculus of Variations*

**DR SIMUKAI UTETE**
*Academic Director and Senior Resident Researcher*

**PROF IAN DURBACH**
*Associate Research Fellow*
*Department of Statistical Sciences, UCT*


**DR NADEEM OOZEER**
*Associate Research Fellow*
*SKA South Africa*

**DR SHANKAR AGARWAL**
*Postdoctoral Fellow*
*Data Science*


**DR EMMANUEL DUFOURQ**
*Postdoctoral Fellow*
*Deep Learning - Ecological Problems*

**DR DANIEL NICKELSON**
*Postdoctoral Fellow*
*Theoretical Physics*

**DR MILAINE TCHAMGA**
*Postdoctoral Fellow*
*Biomathematics*

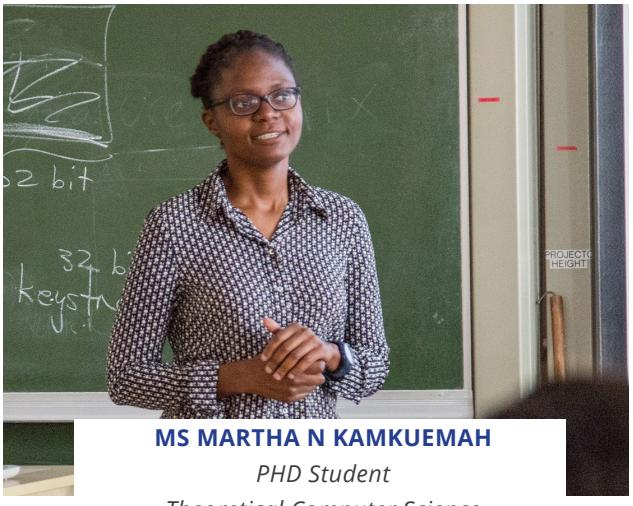

**MS MARTHA N KAMKUEMAH**
*PHD Student*
*Theoretical Computer Science*

**MS ROJO FANAMPERANA RANDRIANOMENTSOA**
*Research Master's Student*

## Contact Us:


AIMS SOUTH AFRICA RESEARCH CENTRE

5 Melrose Road

Muizenberg

Cape Town 7495

South Africa

TEL: +27 (0)21 787 9320

EMAIL: research-admin@aims.ac.za

WEB: www.aims.ac.za



science & technology
Department:
Science and Technology
REPUBLIC OF SOUTH AFRICA

NRF National Research Foundation

Federal Ministry of Education and Research

Alexander von Humboldt Stiftung/Foundation

DAAD

IDRC | CRDI Canada